
Miikka Mankinen

# Development and Validation of a Hydropower Plant Simulation Model with Hybrid Control

School of Technology and Innovations
Master of Science in Technology
Master's Programme in Smart Energy Transition

Vaasa 2026

**VAASAN YLIOPISTO**
**Tekniikan ja innovaatiojohtamisen akateeminen yksikkö**
**Tekijä:** Miikka Mankinen
**Tutkielman nimi:** Vesivoimalaitoksen hybridisäädöllä varustetun simulointimallin kehittäminen ja validointi
**Tutkinto:** Diplomi-insinööri
**Koulutusohjelma:** Sähkötekniikka
**Työn valvoja:** Hannu Laaksonen
**Työn ohjaajat:** Tapio Karppi, Jukka Prusti, Heikki Istolahti
**Työn tarkastaja:** Kimmo Kauhaniemi
**Valmistumisvuosi:** 2026 **Sivumäärä:** 85

**TIIVISTELMÄ:**
Tässä diplomityössä tarkasteltiin vesivoimalaitoksen hybridisäätäjän simulointimallin kehittämistä ja validointia Kaplan-turbiinilla varustetussa vesivoimalaitoksessa. Työ tehtiin ABB Oy, Energy Industries divisioonalle. Työn tavoitteena oli kehittää DIgSILENT PowerFactory -ohjelmistolla simulointimalli, joka kuvaa vesivoimalaitoksen toimintaa riittävän tarkasti nykyisten pohjoismaisten taajuusohjatun käyttöreservin (FCR) vaatimusten mukaisissa käyttötilanteissa. Työn taustalla on pohjoismaisen sähköjärjestelmän muuttuneet käyttöolosuhteet, kuten uusiutuvan sääriippuvaisen tuotannon lisääntyminen ja sähköjärjestelmän inertian pieneneminen. Nämä ovat kiristäneet reservimarkkinoiden teknisiä suorituskyky- ja vakausvaatimuksia. Työn tavoitteena oli rakentaa ja validoida ABB:n TG800-turbiinisäätäjästä ja Kaplan-turbiinista koostuva simulointimalli todellista mittausdataa vasten sekä tutkia, miten simulointimalliin integroitu energiavarasto voi parantaa laitoksen suorituskykyä reservituotannossa. Työhön sisältyy myös simulointeja, joilla tutkittiin, voidaanko integroidun energiavaraston avulla vähentää johtopyörän ja juoksupyörän liikkeitä FCR-tuotannossa. Toteutetussa simulointimallissa TG800-säätäjä mallinnettiin ABB:n dokumenttien perusteella, ja Kaplan-turbiinimallin toteutuksessa hyödynnettiin olemassa olevaa kirjallisuutta ja tutkimusartikkeleita. Integroidussa hybridimallissa hyödynnettiin DIgSILENTin valmista BESS-pohjaa.

Validointi toteutettiin vaiheittain. Ensimmäisessä vaiheessa validoitiin turbiinimalli vertaamalla simuloitua generaattorin pätötehoa mitattuun dataan FCR-N- ja FCR-D-käyttöönottomittausten avulla. Toisessa vaiheessa validoitiin turbiinisäätäjä, jossa simuloituja johtopyörän ja juoksupyörän asentoja verrattiin mittausdataan. Lopuksi koko malli validoitiin yhtenä kokonaisuutena siten, että malliin syötettiin mittausdatasta FCR-N- ja FCR-D-käyttöönottomittausten taajuussignaalia. Validoinnin tulokset osoittivat, että Kaplan-turbiinimalli sekä TG800-säätäjä kuvasivat vesivoimalaitoksen käyttäytymistä riittävän tarkasti dynaamisia simulointeja varten, vaikka yksittäisissä käyttötilanteissa havaittiin joitakin poikkeamia. Lisäksi työssä tutkittiin simulointimalliin integroidun akkuenergiavaraston vaikutusta laitoksen suorituskykyyn ja sen säätömekanismien liikkeisiin. Tulosten perusteella hybridisäätö paransi vesivoimalaitoksen suorituskykyä nykyisten FCR-vaatimusten näkökulmasta. Samalla energiavarasto vähensi merkittävästi vesivoimalaitoksen säätömekanismien liikkeitä. Kahden tunnin FCR-N-simuloinnissa johtopyörän liikkeet vähenivät 88,28 % ja juoksupyörän liikkeet 89,77 %. Johtopäätöksenä todettiin, että hybridisäätö voi auttaa hitaan dynamiikan vesivoimalaitoksia täyttämään nykyiset FCR-vaatimukset ja samalla vähentämään mekaanista kulumista niiden säätömekanismeissa.

**AVAINSANAT:** Hybridisäätö, simulointimalli, vesivoima, reservimarkkinat, validointi

**UNIVERSITY OF VAASA**
**School of Technology and Innovations**
**Author:** Miikka Mankinen
**Title of the thesis:** Development and Validation of a Hydropower Plant Simulation Model with Hybrid Control
**Degree:** Master of Science
**Programme:** Electrical Engineering
**Supervisor:** Hannu Laaksonen
**Intructors:** Tapio Karppi, Jukka Prusti, Heikki Istolahti
**Evaluator:** Kimmo Kauhaniemi
**Year:** 2026 **Pages:** 85

**ABSTRACT:**
This master's thesis examined the development and validation of the simulation model of a hybrid controller in a hydropower plant equipped with a Kaplan turbine. The work was carried out for ABB Oy, Energy Industries division. Its objective was to develop, with DIgSILENT PowerFactory software, a simulation model that describes the operation of the hydropower plant in operating situations compliant with the current Nordic requirements for Frequency Containment Reserve (FCR). In the background of the work were the changed operating conditions of the Nordic power system, such as the increase in weather-dependent renewable production and the decrease in the inertia of the power system. These have tightened the technical performance and stability requirements of the reserve market. The objective of the work was to build and validate a simulation model consisting of ABB's TG800 turbine governor and a Kaplan turbine against real measurement data, and to investigate how an energy storage system integrated into the simulation model can improve the plant's performance in reserve production. The study also includes simulations that examined whether the integrated energy storage system can reduce guide vane and runner blade movements in FCR production. In the simulation model, the TG800 governor was modeled based on ABB's documents, and in the implementation of the Kaplan turbine model, existing literature and research articles were utilized. In the integrated hybrid model, DIgSILENT's pre-built BESS template was utilized.

The validation was carried out in stages. In the first stage, the turbine model was validated by comparing the simulated generator active power with measured data by means of FCR-N and FCR-D site measurements. In the second stage, the turbine governor was validated, in which the simulated guide vane and runner blade positions were compared with measurement data. Finally, the complete simulation model was validated so that the frequency signal of the FCR-N and FCR-D site measurements from the measurement data was fed into the model. The results of the validation showed that the Kaplan turbine model and the TG800 governor described the behaviour of the hydropower plant with sufficient accuracy for dynamic simulations, although some deviations were observed in individual operating situations. Also, the work investigated the influence of the battery energy storage system integrated into the simulation model on the plant's performance and on the movements of its control mechanisms. Based on the results, hybrid control improved the performance of the hydropower plant from the perspective of the current FCR requirements. At the same time, the energy storage system significantly reduced the movements of the hydropower plant's control mechanisms. In the two-hour FCR-N simulation, the guide vane movements decreased by 88.28% and the runner blade movements by 89.77%. As a conclusion, it was stated that hybrid control can help hydropower plants with slow dynamics fulfil the current FCR requirements and at the same time reduce mechanical wear and tear in their control mechanisms.

**KEYWORDS:** Hybrid controller, simulation model, hydropower, reserve markets, validation

## Preface

This thesis gave me a unique opportunity to gain experience in simulation, hydropower technology, electricity reserve markets, and academic thinking. During the thesis, I was more or less thrown in at the deep end in nearly every area related to the topic, and I am truly grateful for everything it has given me.

I would like to thank ABB Oy, Energy Industries division, for this great opportunity to carry out my master's thesis. I would also like to thank my supervisors, Tapio Karppi, Heikki Istolahti, and Jukka Prusti, as well as all the colleagues who supported me throughout the process. Special thanks go to Jukka Prusti for his enthusiasm, expertise, and valuable advice and guidance throughout the work.

Finally, I would like to thank my family, friends, and loved one for their support and patience throughout this five-year journey.

Vaasa, 7th May 2026

Miikka Mankinen

## Contents

## Figures

## Tables



## ABBREVIATIONS

| | |
|---|---|
| ABB | Asea Brown Boveri |
| AC | Alternating Current |
| aFFR | Automatic Frequency Restoration Reserve |

| | |
|---|---|
| AVR | Automatic Voltage Regulator |
| BESS | Battery Energy Storage System |
| CHP | Combined Heat and Power |
| DSL | DIgSILENT Simulation Language |
| DSO | Distribution System Operator |
| EU | European Union |
| EU ETS | European Union Emissions Trading System |
| EV | Electric Vehicle |
| FCR | Frequency Containment Reserve |
| FCR-D | Frequency Containment Reserve for Disturbances |
| FCR-N | Frequency Containment Reserve for Normal Operation |
| FFR | Fast Frequency Reserve |
| FSM | Frequency Sensitive Mode |
| GV | Guide Vane |
| HTG800 | Hydro Turbine Governor 800 |
| Hz | Hertz |
| LFSM-O | Limited Frequency Sensitive Mode - Overfrequency |
| LFSM-U | Limited Frequency Mode - Underfrequency |
| mFRR | manual Frequency Restoration Reserve |
| MVA | Megavolt-ampere |
| MW | Megawatt |
| NAG | Nordic Analysis Group |
| PID | Proportional-Integral-Derivative |
| PI | Proportional-Integral |
| p.u | per unit |
| RB | Runner Blade |
| RoCoF | Rate of Change of Frequency |
| RMS | Root Mean Square |
| SciPy | Scientific Python |
| TSO | Transmission System Operator |

## Symbols & Greek and Roman letters

| | |
|---|---|
| $A$ | Pipe area |
| $a_g$ | Acceleration due gravity |
| $A_t$ | Turbine gain |
| $B_{flow}$ | Gain representing blade angle impact |
| $D_{hybrid}$ | Total movement with hybrid control |
| $D_{n\text{-}hybrid}$ | Total movement without hybrid control |
| $e(t)$ | Control error |
| $Ep$ | Droop |
| $f$ | Frequency |
| $f(y)$ | Function describing the guide vane position relationship |
| $f(y_r)$ | function describing the runner blade position relationship |
| $f_0$ | Nominal frequency |
| $G$ | Ideal gate opening and turbine control signal |
| $g$ | Real gate opening |
| $g_{FL}$ | Full-load gate opening |
| $g_{NL}$ | No-load gate opening |
| $H_{sys}$ | Inertia constant of power system |
| $H$ | Hydraulic head at gate |
| $H_0$ | Initial steady-state value of hydraulic head |
| $h_0$ | Steady-state head |
| $H_r$ | Rated hydraulic head |
| $j$ | Imaginary unit |
| $K$ | PI controller parameter |
| $K_d$ | Derivative gain |
| $K_i$ | Integral gain |
| $K_p$ | Proportional gain |
| $K_u$ | Constant of proportionality in turbine water velocity equation |
| $L$ | Length of conduit |

| | |
|---|---|
| $MVA_{base}$ | The reference MVA used as the base value for expressing the turbine torque in per-unit value |
| $P$ | Turbine power |
| $P_m$ | Mechanical power |
| $P_r$ | Turbine rating |
| $P_{ss,0}$ | Steady-state power before the first step |
| $P_{ss,1}$ | Steady-state power during the first step |
| $P_{ss,2}$ | Steady-state power during the second step |
| $P_{ss,3}$ | Steady-state power during the third step |
| $P_{LOAD}$ | Total load of the power system |
| $Q$ | Water flow rate |
| $q_0$ | No-load turbine flow |
| $s$ | Laplace variable |
| $T$ | PI controller parameter |
| $t$ | Time in seconds |
| $T_{feedback}$ | Feedback time constant |
| $T_i$ | Integral time |
| $T_w$ | Water time constant |
| $U$ | Water velocity |
| $u(t)$ | Controller output signal |
| $U_r$ | Rated water velocity |
| $y$ | Guide vane position variable |
| $y_r$ | Runner blade position variable |
| $b_0$ | Polynomial coefficient of the guide vane fitting function |
| $b_1$ | Polynomial coefficient of the guide vane fitting function |
| $b_2$ | Polynomial coefficient of the guide vane fitting function |
| $b_3$ | Polynomial coefficient of the guide vane fitting function |
| $b_4$ | Polynomial coefficient of the guide vane fitting function |
| $b_5$ | Polynomial coefficient of the guide vane fitting function |
| $\Delta E_{7.5s}$ | Activated energy during first 7.5 seconds |

| | |
|---|---|
| $\Delta P(t)$ | Change in contributed power |
| $\Delta P_{7.5s}$ | Power response at 7.5 seconds |
| $\Delta P_{imbalance}$ | Active power imbalance |
| $\Delta P_{ss,1}$ | Upward steady-state active power response |
| $\Delta P_{ss,2}$ | Downward steady-state active power response |
| $\Delta P_{ss,theoretical}$ | Theoretical steady-state response |
| $\omega$ | Angular speed |
| $\omega_0$ | Nominal angular speed |
| $\bar{G}$ | Per-unit ideal gate opening |
| $\bar{H}$ | Per-unit hydraulic head |
| $\bar{H}_0$ | Per-unit steady-state hydraulic head |
| $\bar{P}_m$ | Per-unit mechanical power |
| $\bar{P}_r$ | Per-unit turbine rating |
| $\bar{T}_m$ | Per-unit mechanical torque |
| $\bar{U}$ | Per-unit water velocity |
| $\bar{U}_{NL}$ | Per-unit no-load water velocity |
| $\bar{\omega}$ | Per-unit speed |

# 1 Introduction

The operating environment of the Nordic power system has changed in recent years. Changes in electricity generation such as the increasing share of weather-dependent renewable production and the reduction of system inertia, has increased the requirements for power-system frequency control (Khajeh & Laaksonen, 2022a; Nordic Analysis Group, NAG, 2025). Because of these changes, the technical requirements of the reserve markets have been updated, resulting in stricter demands for faster, more accurate, and more stable responses from entities providing Frequency Containment Reserve (FCR).

Hydropower production plays an important role in the reserve markets because their power output can be regulated flexibly (Schäffer et al., 2023). However, the dynamic behaviour of hydropower plants involves water-related characteristics that complicate compliance with the current FCR requirements. In production units equipped with Kaplan turbines, waterway dynamics, mechanical delays, and control-system settings influence how fast and stable a plant can respond to grid frequency deviations. For this reason, modeling and analysing hydropower plants is important when assessing their ability to meet the current requirements for FCR provision.

One potential solution for improving the dynamic performance of a hydropower plant is the integration of an energy storage system. A such system can participate to the plant's power output during FCR provision, thereby improving its performance while also reducing the mechanical wear and tear of turbine components caused by continuous regulation (Feng et al., 2024). This master's thesis combines the FCR requirements developed in cooperation between the Nordic Transmission System Operator (TSOs): Energinet, Fingrid, Stattnet and Svenska kraftnät with the dynamic modeling of hydropower plant and the application of hybrid control. In this thesis, a simulation model is developed using the PowerFactory software and later validated. Based on the validated simulation model, it becomes possible to examine how accurately it represents the dynamics of the actual

hydropower plant and what benefits an integrated energy storage system can provide in continuous frequency control.

## 1.1 Problem Formulation

As the needs of the Nordic synchronous area's power system evolve, the new requirements imposed on participants in the electricity reserve markets are becoming stricter and, therefore, more challenging to meet than the old standards. Some of the existing providers of FCR may be unable to comply with the updated requirements, or their available production capacity in FCR market may decrease as a result of these changes.

In the Nordic countries, FCR is produced through various means, with hydropower representing a key sector. However, hydropower plants may face difficulties in meeting the new requirements due to their slow dynamics. The hydraulic characteristics of hydropower can lead to challenges in achieving the required response times and maintaining stability in grid disturbance scenarios (*Explanatory Document*, n.d.). This is particularly relevant for Finnish hydropower plants, as they are often run-of-river plants with low heads and high flow rates.

## 1.2 Research Questions

These research questions were derived from the problem formulation, which highlighted the challenges faced by hydropower plants because of the updated requirements in the FCR markets. The purpose of these questions was to identify the root causes of the problem.

**Question 1:**

How accurately does the developed PowerFactory simulation model represent the dynamic behavior of a hydropower plant when validated against site measurement data?

**Question 2:**

How does a BESS integrated into the simulation model's turbine governor affect the power response and stability of a hydropower plant with a slow dynamic response?

**Question 3:**

How much can guide vane and runner blade movements be reduced by integrating a BESS into the turbine governor during FCR-N provision?

## 1.3 Scope of the Work

The primary focus of this thesis is to develop a simulation model of a hydropower plant hybrid governor for ABB Oy, Energy Industries division. The model is implemented using the DIgSILENT PowerFactory software, and the work focuses on modeling the Kaplan turbine and turbine governor as part of the hybrid controller. In addition, the turbine governor and turbine model developed as part of the simulation model are tested and validated using measurement data provided by a Finnish hydropower company. The purpose of the work is to create an accurate simulation model suitable for dynamic simulations and to be compliant to simulate according to current FCR requirements.

The objective of the simulations is to validate the developed turbine governor and turbine model primarily through Root Mean Square (RMS) simulations using real operational data from a hydropower plant. The simulation results are then compared with the actual behavior of the plant obtained from site measurement tests. A further objective is to assess how the integration of an energy storage system could improve the turbine's power output and response time during FCR provision.

## 1.4 Expected Results

Based on the simulations to be conducted in this study, it is hypothesized that the hybrid controller, with an integrated energy storage system, could participate in power generation during grid disturbances and FCR provision, thereby reducing the hydropower plant's power output response time in the event of a frequency deviation in the grid. It is also assumed that the inclusion of an energy storage system would enhance the stability of the hydropower plant's power output. Finally, it is hypothesized that the integrated energy storage system would assist in the fine-tuning of the turbine's operation, thereby reducing mechanical wear and tear on its components.

Given the expected technical outcomes, expectations for economic profitability are notable. With faster and higher-quality power output, the plant could increase its participation share in the FCR markets, while the reduced mechanical control demand could extend the intervals between maintenance operations or at least lower the costs associated with necessary repairs. However, economic profitability is excluded from this study.

# 2 Operation of the Finnish Transmission System

This chapter provides a general overview of the operation of the Finnish power transmission system, with a particular focus on frequency control and the factors influencing it. A system-level understanding of frequency regulation, overall system operation, and reserve provision is essential when considering hydropower production as part of a power transmission system. First, the role and responsibilities of the Finnish TSO are discussed. This is followed by a discussion of the current and future challenges facing the power system, with particular focus on issues related to frequency deviation. Finally, technical requirements related to reserve market participation are reviewed.

## 2.1 Principles of Finnish Transmission System Operation

The Finnish transmission grid is managed by the TSO Fingrid Oyj, which is owned by Finnish pension insurance companies and the State of Finland. Fingrid's mission is to ensure the reliable operation of Finland's electricity transmission network and to promote a clean, market-driven electricity system. The transmission grid system maintained by Fingrid consists of high-voltage transmission lines forming a meshed backbone network that connects major power plants, industrial facilities, and distribution networks. In 2023, Finland's transmission grid consisted of approximately 14,500 kilometers of power lines and more than 120 substations. Fingrid is also part of the Nordic power system, referred to as the Nordic synchronous area. A synchronous area is an area in which all interconnected electricity networks function in synchronism through alternating current (AC) connections. Alongside Finland, the Nordic synchronous area includes Sweden, Norway, and eastern Denmark (*Electricity System of Finland*, n.d).

To ensure secure power system operation, all production facilities connected to the grid managed by Fingrid are required to comply with its own Grid Code Specifications for Power Generating Facilities. These specifications are based on the European Network

Code (EU Commission Regulation 2016/631), to which Fingrid has added national additions and clarifications. The purpose of the Grid Code Specifications (VJV2024) is to ensure that generating units remain stable during voltage and frequency deviations, support the power system during faults, avoid harmful effects on other connected equipment, and provide the information needed for network planning, operation, and system security (*Grid Code Specifications for Power-Generating Facilities VJV2024*, n.d.).

One of the main factors in secure power system operation is frequency. Frequency control is influenced by several factors, the most significant is the balance between electricity production and consumption. Frequency is measured in Hertz (Hz), which represents the number of alternating current periods per second. The Nordic power system is designed to operate at a nominal frequency of 50 Hz, however, the actual frequency deviates around the power system's nominal frequency where deviation of 0.1 Hz is considered as a small deviation during normal operation. These deviations are mostly caused by imbalances between production and consumption. In addition, frequency deviation is affected by system inertia, which acts as a buffer that slows down frequency changes and corresponds to the kinetic energy stored in the synchronous generators connected to the power system (entsoe, 2022).

For frequency support, the TSO obtains technical services through the technical ancillary service markets. These consist primarily of Frequency Containment Reserves (FCR), Fast Frequency Reserve (FFR), and Frequency Restoration Reserves (aFRR and mFRR), which operate on different time scales during frequency deviations. The technical ancillary service markets enable the technical stability and operational reliability of the power system under both normal and disturbed operating conditions (Khajeh & Laaksonen, 2022b).

## 2.2 Current and Future Challenges of the Finnish Power System

Current challenges in power system frequency control include an increasing need for regulation, limited flexibility capacity, and a growing demand for flexibility across different voltage levels. In Finland, the increasing need for regulation is driven by several factors, including the reduced profitability of combined heat and power (CHP) plants due to declining electricity prices and rising prices in the EU Emissions Trading System (EU ETS). This has led CHP plants to increasingly utilize large-scale heat pumps and electric boilers for heat production. In addition, the growing appearance of extreme weather conditions and the high number of unplanned outages experienced by nuclear power plants further contribute to the rising regulation demand (Koivunen & Syri, 2024).

The balance of the power system is also influenced by several other factors, such as the expansion of the grid infrastructure, the intensification of extreme weather events, large-scale power transfers from the edges of the grid toward its center, and market dynamics. Another aspect to consider is the impact of the increasing use of power electronics on load behavior.

In the future, the power system relies more on weather-dependent renewable energy production, causing a growing need for effective frequency control. At the Distribution System Operator (DSO) level, these effects will strengthen alongside the increasing demand for electric vehicle (EV) charging. This development may result in voltage limit violations and congestion within distribution networks. These issues are also relevant at the TSO level, where system-wide imbalances between production and consumption must be managed (Khajeh & Laaksonen, 2022b).

In addition to local voltage and congestion challenges at the DSO level, one of the most critical system-level challenges influencing frequency stability is the reduction of overall system inertia. Power system inertia originates from the kinetic energy stored in the rotating masses of synchronous machines. It represents the system's ability to resist frequency changes in the event of a sudden disturbance, such as a fault in a large

production unit. These frequency changes, known as RoCoF, can be mathematically expressed by

$$RoCoF|_{t=0^+} = \frac{\Delta P_{imbalace} f_0}{P_{LOAD} 2H_{sys}}, \quad (1)$$

where *RoCoF 0⁺* represents the time derivative of the power system frequency at the exact moment when the disturbance occurs, $\Delta P_{imbalance}$ is active power imbalance, $P_{LOAD}$ is the total load of the system, $f_0$ is the nominal frequency and $H_{sys}$ is the inertia constant (*Inertia and Rate of Change of Frequency*, n.d.). Equation (1) shows the RoCoF during a system disturbance and shows that the system inertia is inversely proportional to the RoCoF value. Therefore, when the power system inertia decreases, the RoCoF increases even if the magnitude of the disturbance remains the same.

The higher the RoCoF value, the faster the system frequency drops towards the critical threshold of 49.0 Hz during a disturbance. This requires that frequency reserves respond faster and more effectively to prevent load shedding at 48.8 Hz or the automatic disconnection of generators caused by under-frequency conditions (Nordic Analysis Group, NAG, 2025).

## 2.3 Reserve Markets and Related Products

In an electrical power system, production and consumption must remain continuously balanced, as significant frequency deviations can damage equipment or components connected to the grid. In the worst-case scenario, a major frequency deviation may lead to a widespread power outage. The primary balancing of the power system is achieved through electricity markets, where producers and consumers engage in advance trading where producers sell the electricity they plan to produce, while consumers purchase the electricity they intend to use.

However, production and consumption may deviate from forecasts. Inaccuracies in consumption estimates, weather-dependent production not matching expectations, or faults in power plants and transmission connections can all cause imbalances. Fingrid is responsible for maintaining the balance of Finland's power system and manages potential imbalances in real time using system reserves, which are obtained on a market basis through reserve markets operated by Fingrid. Fingrid purchases reserves from companies capable of adjusting their electricity production or consumption according to the needs of the power system. Participation in the reserve markets does not exclude a power plant's involvement in the wholesale electricity market. Reserve resources include power plants, consumers, energy storage systems, and aggregated entities consisting of smaller units.

There are several types of reserve products that together form the reserve market framework. These products range from fast-responding reserves, which react within less than a second to fine-tune the power system, to slower reserves that balance the system over longer periods (Fingrid, 2025). Reserves are needed for every hour of the year. The various reserve products available on Fingrid's reserve markets are illustrated in Figure 1.

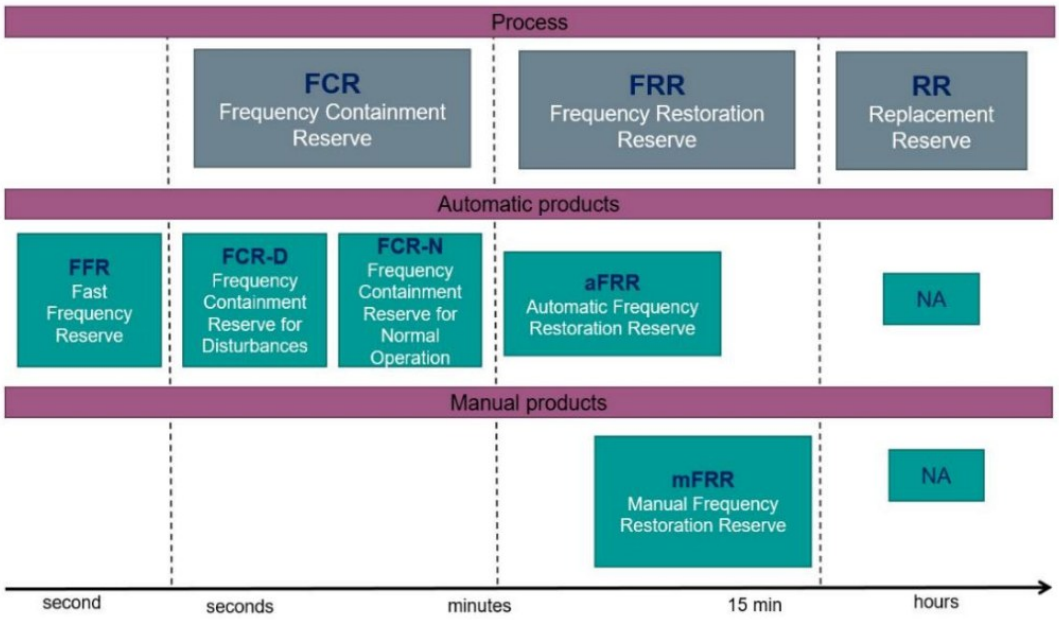


**Figure 1.** Reserve market products in the Nordic countries (Fingrid, 2023).

As mentioned earlier, there are several types of reserve products, each serving a specific purpose. The power grid requires continuous regulation to ensure reliable operation, as well as reserves to address major disturbances in both production and consumption. The following section discusses reserve market products relevant to hydropower, their operating principles, and the requirements for achieving the desired response. Figure 2 illustrates the operating principles of reserve products in a situation where, at time 0 seconds, disturbance situation occurs.

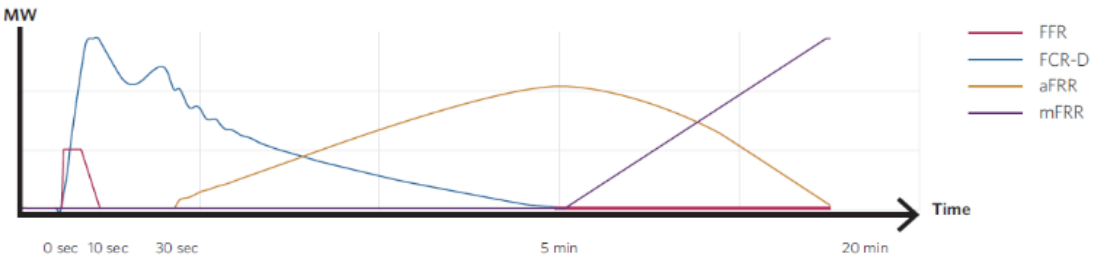


**Figure 2.** Operating principles of reserve products (entsoe, 2022).

Each reserve product is subject to specific technical requirements regarding activation time, minimum bid size, and stability requirement. However, the product requirements have undergone changes, especially regarding transient and small signal frequency stability. As a result, reserve providers must update their systems to comply with the new requirements established by the nordic TSOs.

The Nordic TSOs have implemented a five-year transitional period starting in 2023 concerning the new requirements. This means that all reserve providers who validated their facilities in accordance with the TSOs' requirements before 2023 are allowed to participate in the reserve markets until 2028, by which time their systems must be updated. If a reserve provider wishes to modify its product during this period, it must undergo validation in accordance with the new requirements. The new requirements established by the TSOs are currently in effect as the current requirements (Nordic Analysis Group, NAG, 2025). The following sections examine in greater detail why updates to the reserve product requirements are necessary and how these changes practically affect the modeling and design of reserve products, especially from the perspective of hydropower plants.

## 2.4 Technical Requirements for FCR Products

This section summarizes the technical requirements for the FCR-N, FCR-D Up, and FCR-D Down products. Rather than reproducing all requirements specified in document (Gierling, 2025), the focus is limited to those requirements that are used for validating the turbine-governor and turbine model developed in this thesis. For hydropower plants equipped with Kaplan turbines, the requirements that are typically the most demanding from a dynamic performance perspective are therefore examined in greater detail in the following Subsections. The selected requirements are consistent with (Gierling, 2025) and are later used as reference values for the analysis presented in this thesis work.

### 2.4.1 Overview of FCR Products and Required Tests

FCR refers to frequency-controlled reserves that are automatically activated in response to frequency deviations. Within the scope of this thesis, the analysis is limited to the three relevant products: FCR-N, FCR-D Up and FCR-D Down. Table 1 presents the activation characteristics of these FCR products. Where negative activation refers to a reduction in production or an increase in load, while positive activation refers to an increase in production or a reduction in load.

**Table 1.** Steady-state activation of the FCR products (Gierling, 2025).

| **Product** | **100 % negative activation** | **0 % activation** | **100 % positive activation** |
|---|---|---|---|
| FCR-D upward | N.A. | $f \geq 49.9$ Hz | $f \leq 49.5$ Hz |
| FCR-N | $f \geq 50.1$ Hz | $f = 50$ Hz | $f \leq 49.9$ Hz |
| FCR-D downward | $f \geq 50.5$ Hz | $f \leq 50.1$ Hz | N.A. |

A reserve provider must comply with all technical requirements associated with the specific reserve product offered. Table 2 presents these requirements for each product. In the table, the “x” mark indicates the reserve product to which the respective test applies.

**Table 2.** Summary of required tests: Modified from source (Gierling, 2025).

| **Test** | **FCR-N** | **FCR-D Up** | **FCR-D Down** |
|---|---|---|---|
| Steady-state response | x | x (fast ramp) | x (fast ramp) |
| Power after 7,5 s | | x | x |
| Energy 0-7,5 s | | x | x |
| Deactivation | | x | x |
| Frequency domain stability | x | x | x |
| Frequency domain performance | x | x | x |
| Dynamic linearity | x | x | x |

| | | | |
|---|---|---|---|
| Endurance | x | x | x |
| Mode shifting | | x | x |

### 2.4.2 Steady-state Response

The FCR-N steady-state response test is performed by applying a stepwise test signal. The initial step is used to establish the starting condition, ensuring that any effects of mechanical backlash influence the response in the same manner as in the following two steps. Next, the power output must settle at a frequency of 50.0 Hz for five minutes, after which the next step can be applied. Table 3 presents the individual steps of the step test, and Figure 3 illustrates the test using an example simulation.

**Table 3.** FCR-N step sequence test: Modified from source: (Gierling, 2025).

| **Step number** | **Start time (min)** | **Duration (min)** | **Frequency (Hz)** | **Comment** |
|---|---|---|---|---|
| | 0 | 0.5 | 50.0 | Starting point |
| Pre-step | 0.5 | 0.5 | 49.95 | Small step to handle backlash |
| 0 | 1 | 5 | 50.0 | Step for $f_0$, $P_0$ |
| 1 | 6 | 5 | 49.9 | Step for $f_1$, $P_1$ |
| 2 | 11 | 5 | 50.1 | Step for $f_2$, $P_2$ |
| 3 | 16 | 5 | 50.0 | Step for $f_3$, $P_3$ |
| | 21 | | | End of test |

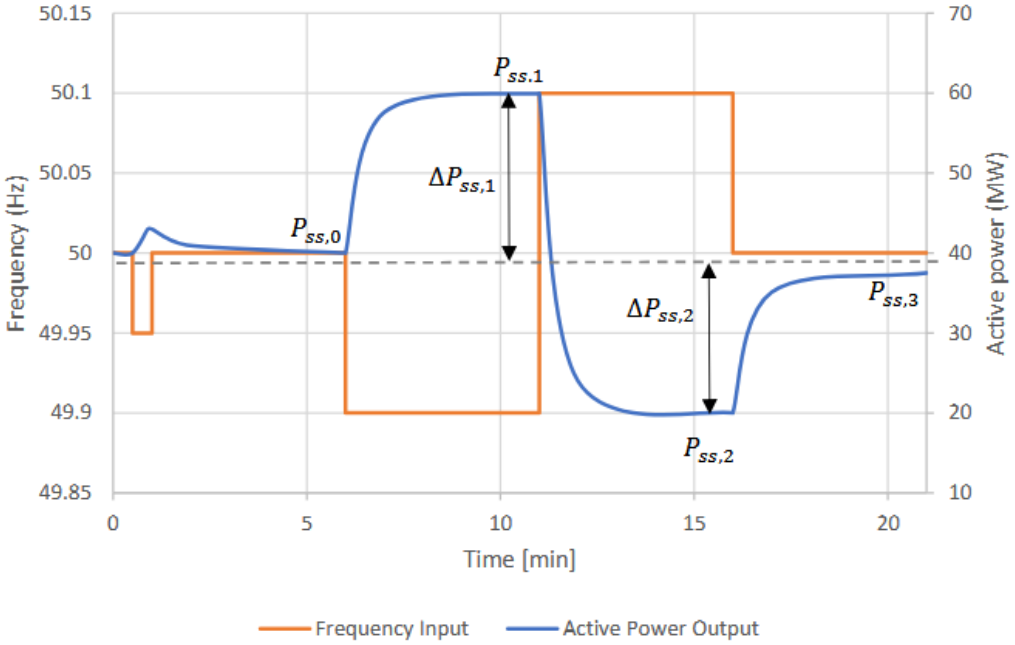


**Figure 3.** FCR-N step sequence test where input frequency (orange) and example response (blue) are shown (Gierling, 2025).

The upward active power shown in Figure 3 can be calculated using the equation

$$\Delta P_{ss,1} = P_{ss,1} - \frac{1}{2}\left(P_{ss,0} + P_{ss,3}\right), \tag{2}$$

and downward active power with equation

$$\Delta P_{ss,2} = P_{ss,2} - \frac{1}{2}\left(P_{ss,0} + P_{ss,3}\right), \tag{3}$$

where the steady-state power $P_{ss,0}$ is before the first step at a frequency of 50 Hz, and the steady-state power $P_{ss,3}$ is after the third step at a frequency of 50 Hz. The steady-state power $P_{ss,1}$ is during the first step at frequency of 49,9 Hz and the steady-state power $P_{ss,2}$ is during the second step at frequency of 50,1 Hz.

Maximum under delivery is 5 % and maximum over delivery is 20 %, upward regulation requirement is defined

$$-0.05 \leq \frac{\Delta P_{ss,1} - \left|\Delta P_{ss,theoretical}\right|}{\Delta P_{ss,theoretical}} \leq 0.2, \quad (4)$$

and downward regulation with equation

$$-0.2 \leq \frac{\Delta P_{ss,2} + \left|\Delta P_{ss,theoretical}\right|}{\Delta P_{ss,theoretical}} \leq 0.05, \quad (5)$$

where $\Delta P_{ss,theoretical}$ presents steady-state response to 0.1 Hz frequency deviation. It is also required that the response is maintained throughout the entire frequency deviation period.

### 2.4.3 Fast Ramp Sequence

For FCR-D, the steady-state response, time domain dynamic performance, and endurance are tested using a ramp sequence. The same test parameters are applied for both upward and downward regulation, with the only difference being the direction of the input frequency signal. Table 4 describes the test duration and the frequency of ramps applied, while Figures 4 and 5 provides a visual representation of the test.

**Table 4.** FCR-D fast ramp tests without endurance and FCR-N/FCR-D combination: Modified from source (Gierling, 2025).

| Ramp no. | Start time (s) | End time ramp (s) | End time test (s) | Ramp speed (Hz/s) | Test duration (s) | Frequency for FCR-D up (Hz) | Frequency for FCR-D down (Hz) |
|---|---|---|---|---|---|---|---|
| | 0 | 0 | 30 | 0 | 30 | 49.9 | 50.1 |
| 1 | 30 | 33.1 | 34.9 | 0.14 | 4.9 | 49.45 | 50.55 |

| | | | | | | | |
|---|---|---|---|---|---|---|---|
| 2 | 34.9 | 39.9 | 90 | 0.09 | 55.1 | 49.9 | 50.1 |
| 3 | 90 | 91.7 | 390 | 0.24 | 300 | 49.5 | 50.5 |
| 4 | 390 | 391.7 | 690 | 0.24 | 300 | 49.9 | 50.1 |
| 5 | 690 | 693.8 | 750 | 0.24 | 60 | 49 | 51 |
| 6 | 750 | 754.2 | 1050 | 0.24 | 300 | 50 | 50 |

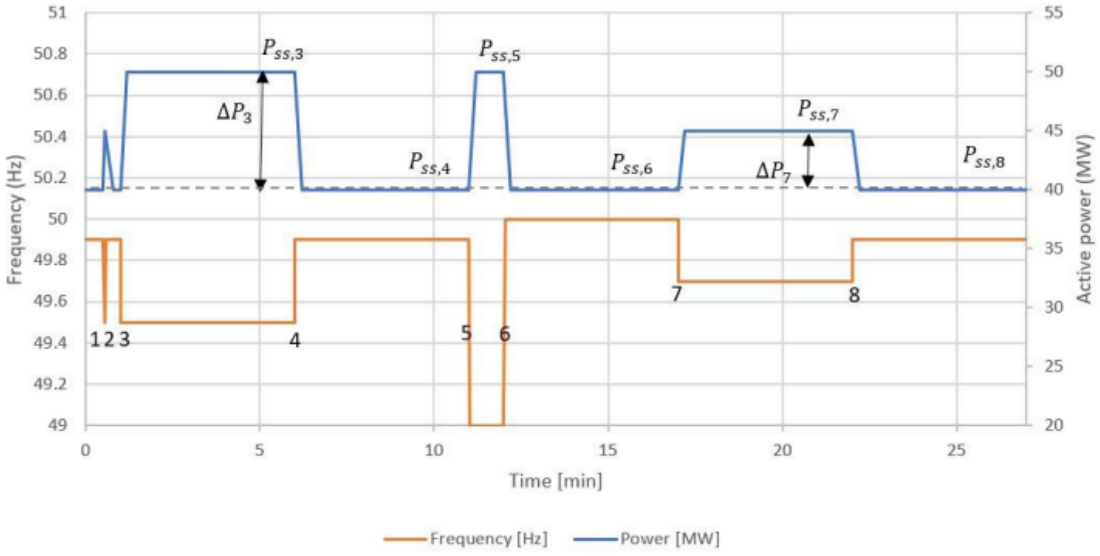


**Figure 4.** FCR-D up regulation (Gierling, 2025).

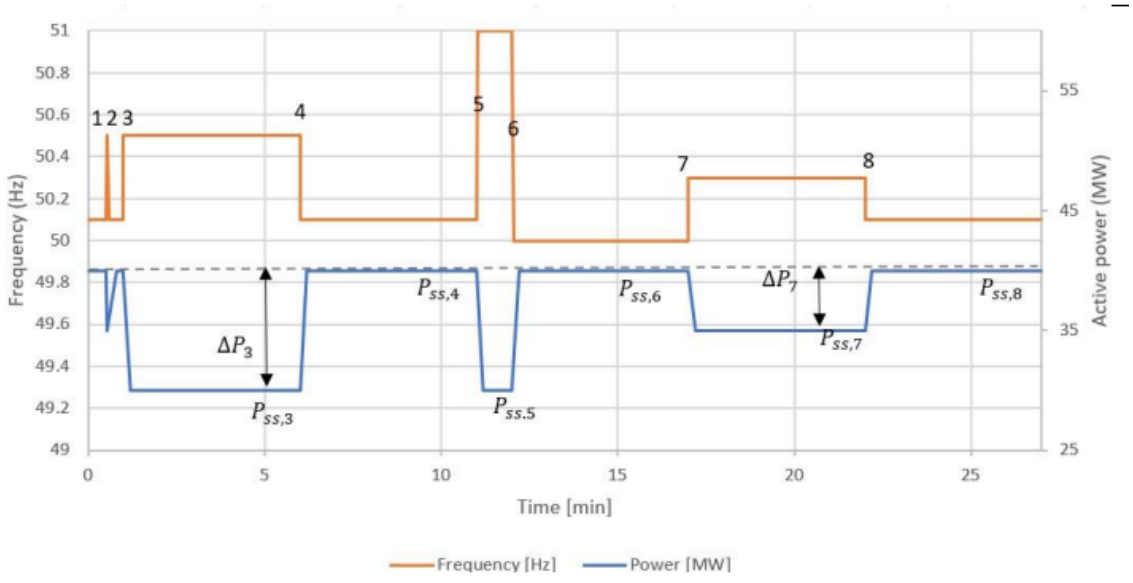


**Figure 5** FCR-D down regulation (Gierling, 2025).

Figure 6 illustrates a typical power response of a Kaplan turbine during ramp 5. Due to the dynamics of the turbine and the waterway, a temporary negative power input response occurs during both upward and downward regulation.

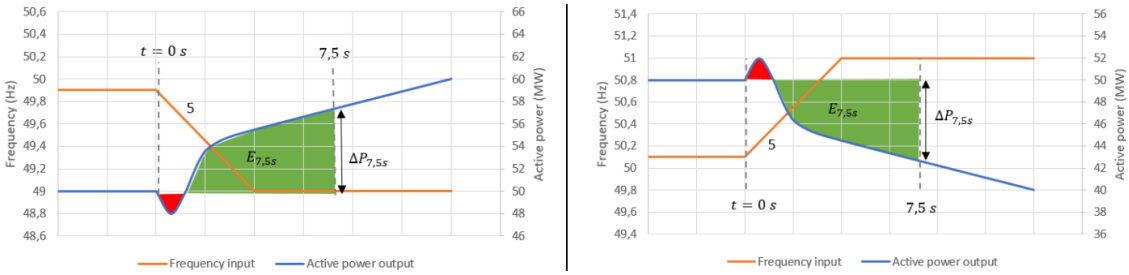


**Figure 6.** Ramp 5 dynamic performance where green area presents positive energy contribution and red area presents negative energy contribution (Gierling, 2025).

The steady-state response of FCR-D is calculated as the difference between the steady-state values of ramps 3 and 4 shown in Figure 5. The maximum allowed under delivery is 5%, and the maximum allowed over delivery is 20%. The upward steady-state response requirement is

$$-0.05 \leq \frac{\Delta P_{ss,3} - P_{ss,4} - \left|\Delta P_{ss,theoretical}\right|}{\Delta P_{ss,theoretical}} \leq 0.2. \quad (6)$$

Similarly to the upward steady-state response, the downward steady-state response requirement is

$$-0.2 \leq \frac{\Delta P_{ss,3} - P_{ss,4} + \left|\Delta P_{ss,theoretical}\right|}{\Delta P_{ss,theoretical}} \leq 0.05, \quad (7)$$

where $\left|\Delta P_{ss,theoretical}\right|$ in megawatts is upward steady-state response between 49.9 Hz and 49.5 Hz, and downward steady-state response between 50.1 Hz and 50.5 Hz calculated using method specified for the provider. The provider must also ensure that the response remains active throughout the entire frequency deviation.

During ramps 5–6 shown in Figures 4 and 5, the provider must also fulfil the power and energy requirements. Requirement for power in megawatts is

$$|\Delta P_{7.5s}| \geq 0.86 \cdot \left|\Delta P_{ss,theoretical}\right|, \quad (8)$$

and the calculated power at 7.5 seconds must not decrease below this value at any point before ramp 6 starts. The small oscillations caused by the 50 Hz test signal applied during ramp 6 are accepted, if they are well damped and originate from the physical characteristics of the provider, such as waterway dynamics.

The energy requirement at 7.5 seconds at ramp 5 is

$$|\Delta E_{7.5s}| \geq 3.2s \cdot \left|\Delta P_{ss,theoretical}\right|, \quad (9)$$

where the activated energy, expressed in megawatt seconds, represents the amount of energy contributed from the start of the ramp until 7.5 seconds. The contributed energy

is obtained by integrating the change in power from the start of the ramp up to 7.5 seconds.

$$E_{7.5s} = \int_{t}^{t+7.5s} \Delta P(t)dt, \tag{10}$$

where $\Delta P$ is change in contributed power and $t$ is the start time of the ramp.

### 2.4.4 Frequency Domain Stability Requirements

Frequency domain stability tests are performed for the FCR-N, FCR-D up, and FCR-D down products. The test consists of sinusoidal tests in which a sinusoidal test signal is superimposed on the nominal frequency, which results in a sinusoidal power output. Test signals with different periods are applied, with a total of ten periods ranging from 10 seconds to 300 seconds depending on the product to be tested. Following Table 5 presents input signals and periods for sine tests to be performed, where period is the time required to complete test signal cycle.

**Table 5.** Sine tests input signals and number of periods: Modified from source (Gierling, 2025).

| **Period *T* (s)** | **N:o stationary periods (recommended total N:o periods)** |
|---|---|
| 10 | 5 (20) |
| 15 | 5 (15) |
| 25 | 5 (10) |
| 40 | 5 (7) |
| 50 | 5 (7) |
| 60 | 5 (7) |
| 70 | 5 (7) |

| | |
|---|---|
| 90 | 5 (7) |
| 150 | 5 (4) |
| 300 | 5 (3) |

Stability is also examined using the Nyquist curve. This curve enables the visualization of closed loop system stability with the open loop transfer function. For example, the poles of a system function

$$H(s) = \frac{P(s)}{Q(s)}, \tag{11}$$

that is, the roots of the denominator polynomial *Q(s),* represent the natural frequencies of the system. If these natural frequencies are located in the left half of the complex s-plane, the system is stable, meaning that its response remains limited. Further discussion on stability can be found in references (Åström & Murray, 2021; Valtonen & Lehtovuori, 2017).

Figure 7 presents an example that passes Nyquist stability criterion. According to the FCR requirements (Gierling, 2025), the system is stable if the Nyquist curve passes the point (-1, 0*j*), where *j* is imaginary unit, on the right side and does not cross over the circle defined around this point.

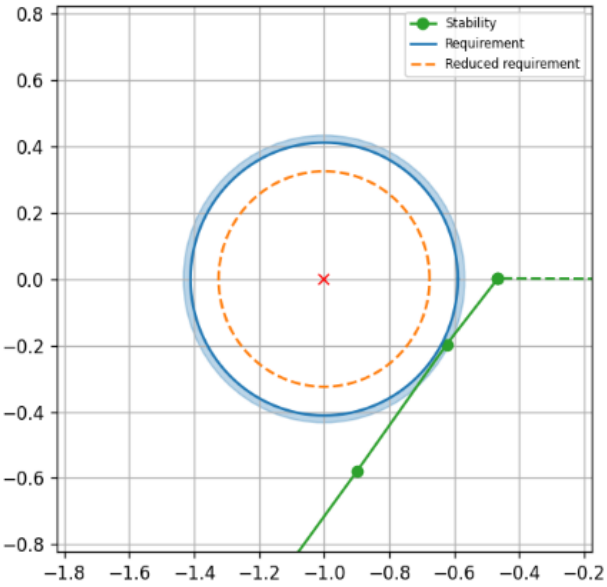


**Figure 7.** Nyquist stability requirement (Gierling, 2025).

# 3 Hydropower and Modeling Principles

A typical hydropower plant consists of several fundamental components and systems, including the high-voltage grid connection, main transformer, cables, protection relays, plant auxiliary systems, hydro turbine, synchronous generator, Automatic Voltage Regulator (AVR), turbine governor and control systems. The following sections focus primarily on the turbine governor system and turbine modeling, as the role of the AVR, generator and other systems are of limited relevance within the scope of this thesis.

## 3.1 Kaplan Turbine Modeling

The Kaplan turbine reminds of a typical propeller in its structural design, and it belongs to the class of reaction turbines. It is typically utilized in electricity production under conditions of low head height and high water flow. To achieve high efficiency, Kaplan turbine applications utilize adjustable Guide Vanes (GV) and Runner Blades (RB), which can be adjusted according to the water flow, head height and the required power output. The flow geometry in a Kaplan turbine is usually axial, meaning that the water moves through the turbine mostly in the direction of the rotor shaft. Figure 8 illustrates a model of the Kaplan turbine. At first, water flows through the penstock into the spiral casing, then through the GV, and later into the RB, causing the turbine shaft to rotate. After passing the RB, the water exits through the conduit.

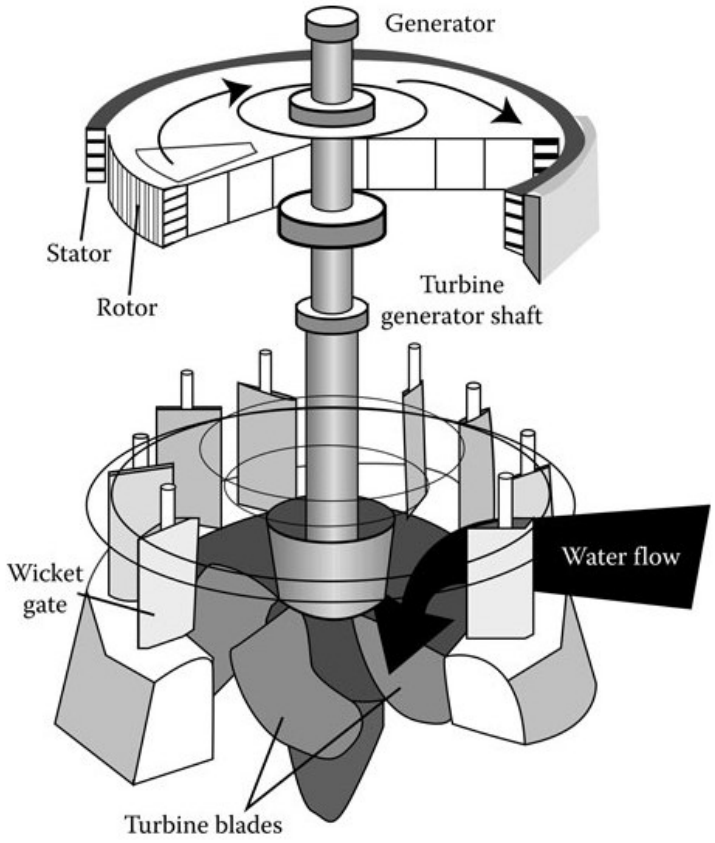


**Figure 8.** Kaplan turbine technical drawing (Grigsby, 2012).

In accurate modeling of Kaplan turbine operation, it is necessary to consider the characteristics of the turbine's penstock and the associated fluid properties. Including water compressibility and the elasticity of the penstock material, which appear in form of travelling waves. The speed of these travelling waves in the penstock are approximately 1200 meters per second, which mean that their effects remain very small unless the penstock is very long. Turbine dynamics and the derivation of the water inertia model are based on Kundur's equations (Kundur, 1994), especially equations (9.1)–(9.36). Equations consider the hydraulic system with inelastic water column and no surge tank. These equations form the basis of the block diagram shown in Figure 9.

Water velocity in the penstock

$$U = K_u G\sqrt{H}. \tag{12}$$

Turbine power

$$P = K_p HU. \tag{13}$$

Expresses that hydraulic power is proportional to head height and water flow. Time derivative of the water velocity in the penstock is

$$\frac{dU}{dt} = -\frac{a_g}{L}(H - H_0). \tag{14}$$

Water flow rate

$$Q = AU, \tag{15}$$

where variables are:

*U* = water velocity

$K_u$ = constant of proportionality

*G* = ideal gate opening

*H* = hydraulic head at gate

$H_0$ = initial steady-state value of *H*

*P* = turbine power

*Q* = water-flow rate

*A* = pipe area

*L* = length of conduit

$a_g$ = acceleration due gravity

*T* = time in seconds

Expression 14 describes how water velocity changes due to deviations in hydraulic head. By expressing variables in per-unit form and dividing by their steady-state values, the normalized equation is

$$\frac{d\bar{U}}{dt} = -\frac{1}{T_w}(\bar{H} - \bar{H}_0). \tag{16}$$

And in Laplace form

$$\frac{\bar{U}}{\bar{H} - \bar{H}_0} = \frac{-1}{T_w s}, \tag{17}$$

where $T_w$ is the water starting time. Expression is at rated load according to turbine's penstock unit expressed as *r*

$$T_w = \frac{LU_r}{a_g H_r}. \tag{18}$$

Hydraulic head can be expressed in per-unit values by dividing equation 12 by its rated values and expressing all variables as in per-unit. This returns to normalized relation

$$\bar{H} = \left(\frac{\bar{U}}{\bar{G}}\right)^2. \tag{19}$$

Turbine power can be expressed as per-unit values in the same manner as hydraulic head by utilizing equation

$$\bar{P}_m = (\bar{U} - \bar{U}_{NL})\bar{H}. \tag{20}$$

From the above equation, the turbine's mechanical power is expressed in per-unit form, which is equal to the turbine's megawatt rating. In stability analysis, the mechanical

torque of the turbine must be expressed in per-unit values, which requires normalization either to the generator's MVA rating or to a separately defined common MVA base. It can be expressed as follows

$$\bar{T}_m = \left(\frac{\omega_0}{\omega}\right)\bar{P}_m\left(\frac{P_r}{MVA_{base}}\right) = \frac{1}{\bar{\omega}}(\bar{U} - \bar{U}_{NL})\bar{H}\bar{P}_r, \tag{21}$$

where variables are:

$\bar{\omega}$ = per unit speed

$MVA_{base}$ = the reference MVA used as the base value for expressing the turbine torque in per-unit value

$\bar{P}_r$ = per unit turbine rating which can be obtained by dividing turbine MVA rating with base MVA value

Turbine gain $A_t$ is defined as the inverse of the difference between full load and no-load gate opening which returns linear relation between ideal real gate positions

$$A_t = \frac{1}{\bar{g}_{FL} - \bar{g}_{NL}}. \tag{22}$$

Ideal gate opening can be expressed with multiplying real gate opening with turbine gain value

$$\bar{G} = A_t\bar{g}. \tag{23}$$

Using equations (12)–(23), the turbine and water column characteristics can be represented completely. This allows the system to be expressed as a block diagram in which turbine control is implemented using the real gate opening together with the turbine gain formulas given in equations (22) and (23). This corresponds to the classical turbine model, which utilizes a single control system. Block diagram is shown in Figure 9.

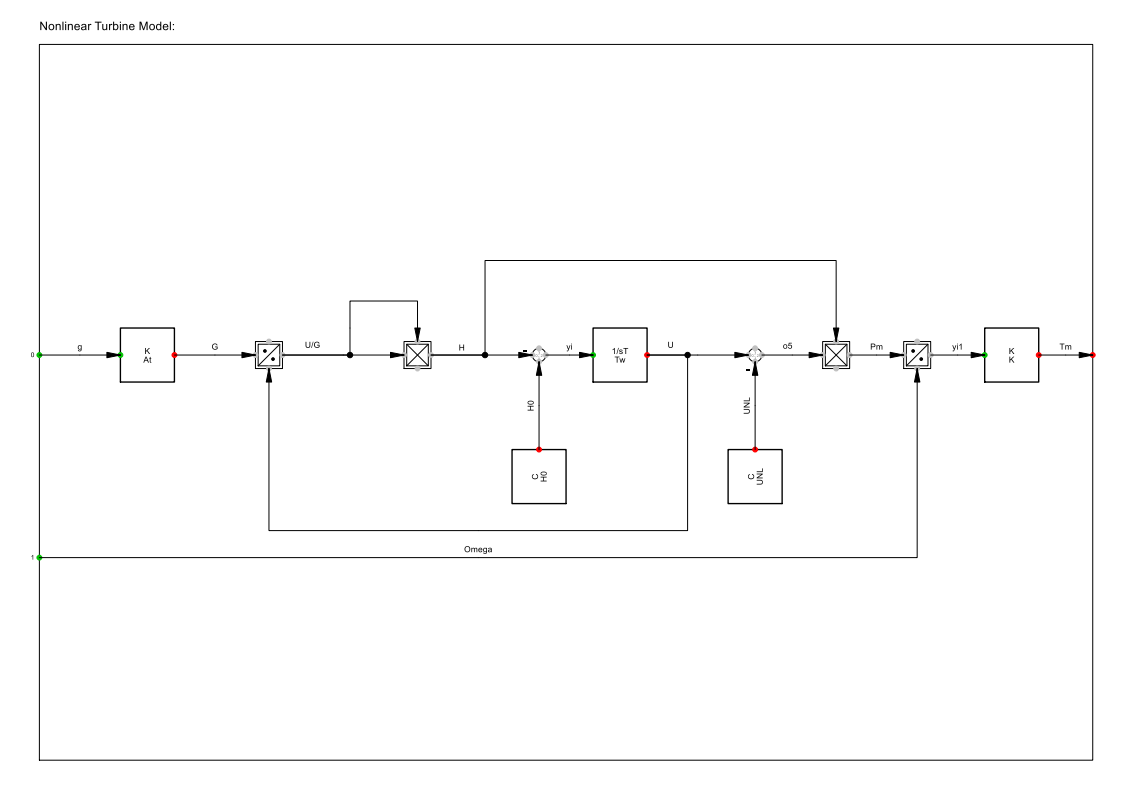


**Figure 9.** Ideal nonlinear turbine block diagram with inelastic water column (Kundur, 1994).

## 3.2 Turbine Control Methods

The fundamental principle of turbine control is to regulate the rotational speed of the turbine and/or the load. Mainly, the control action is based on feedback of the speed error, which is used to adjust the water flow for the turbine (Kundur, 1994). To achieve the highest possible efficiency, a control strategy is required that adjusts the GV and RB positions with respect to the desired turbine power output, thereby forming the control input signal $\bar{G}$. This section reviews the fundamental principles of turbine control and the controller types most relevant to the scope of this thesis. Overview of the turbine and the governor block diagram are shown in Figure 10.

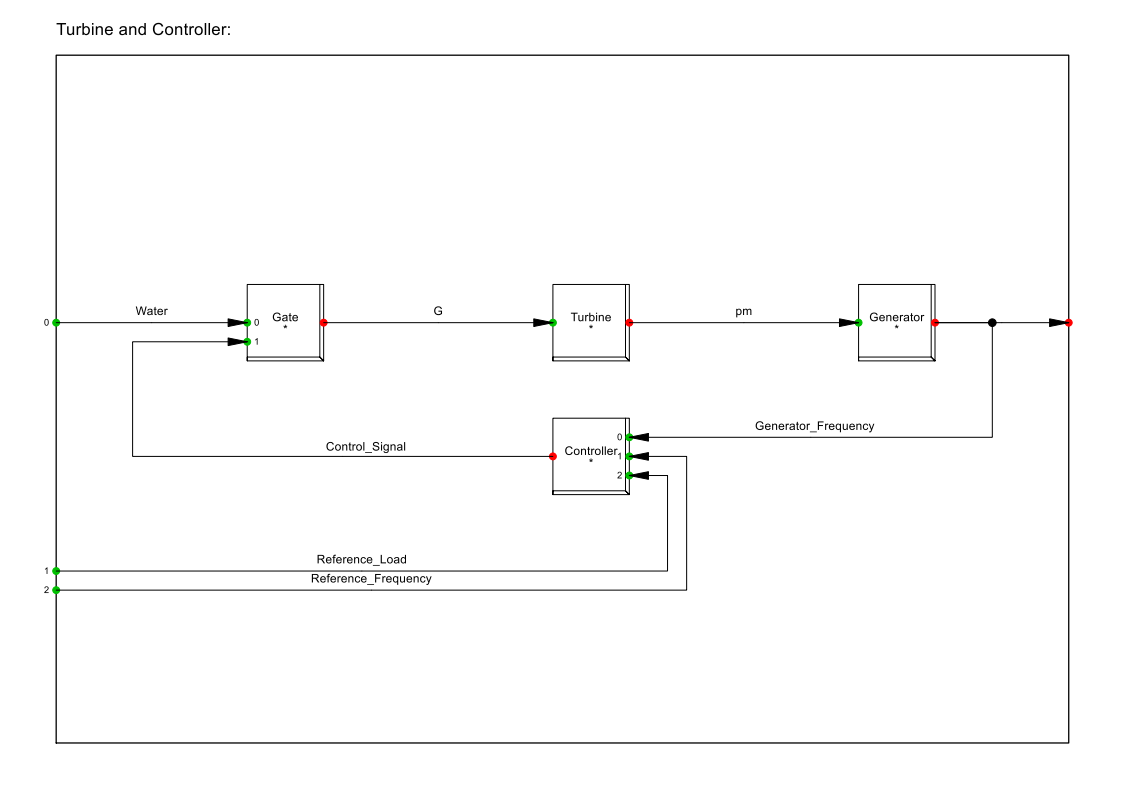


**Figure 10.** Turbine and Controller block diagram overview: Modified from source (Kundur, 1994).

A commonly used feedback-based controller is the PID controller (Åström & Murray, 2021). The control signal *u(t)* is formed as the sum of the proportional *P*, integral *I*, and derivative *D* components as follows:

$$u(t) = K_p e(t) + K_i \int_0^t e(t)dt + K_d \frac{de}{dt}. \tag{24}$$

A PID controller is used to achieve a fast dynamic response through transient gain reduction and transient gain increase. In the PID controller, the derivative term is beneficial in isolated operation and in turbines with high waterway inertia, that is, when the water starting time $T_w \geq 3$ seconds. However, a disadvantage of the derivative term is that it may cause oscillations and instability when the turbine is connected to a strong

interconnected power system. For this reason, the derivative part is typically set to zero. Without the derivative part, the control strategy reduces to a PI controller as follows:

$$u(t) = K_p e(t) + K_i \int_0^t e(t)dt, \tag{25}$$

where the proportional and integral gains can be selected to obtain the desired droop characteristic and recovery time (Kundur, 1994). Since the use of a derivative term is not mandatory for grid-connected hydropower plants, the focus is placed on the PI controller.

Fingrid's guideline document (Nordic Analysis Group, 2023) provides instructions for PI controller tuning with respect to stability margins and performance requirements. The PI controller with droop shown in Figure 11 can be defined using the 63% step response criterion, where the feedback time constant is taken as the moment when the step response has reached 63 % of its final value when gain $K_p$ is ignored.

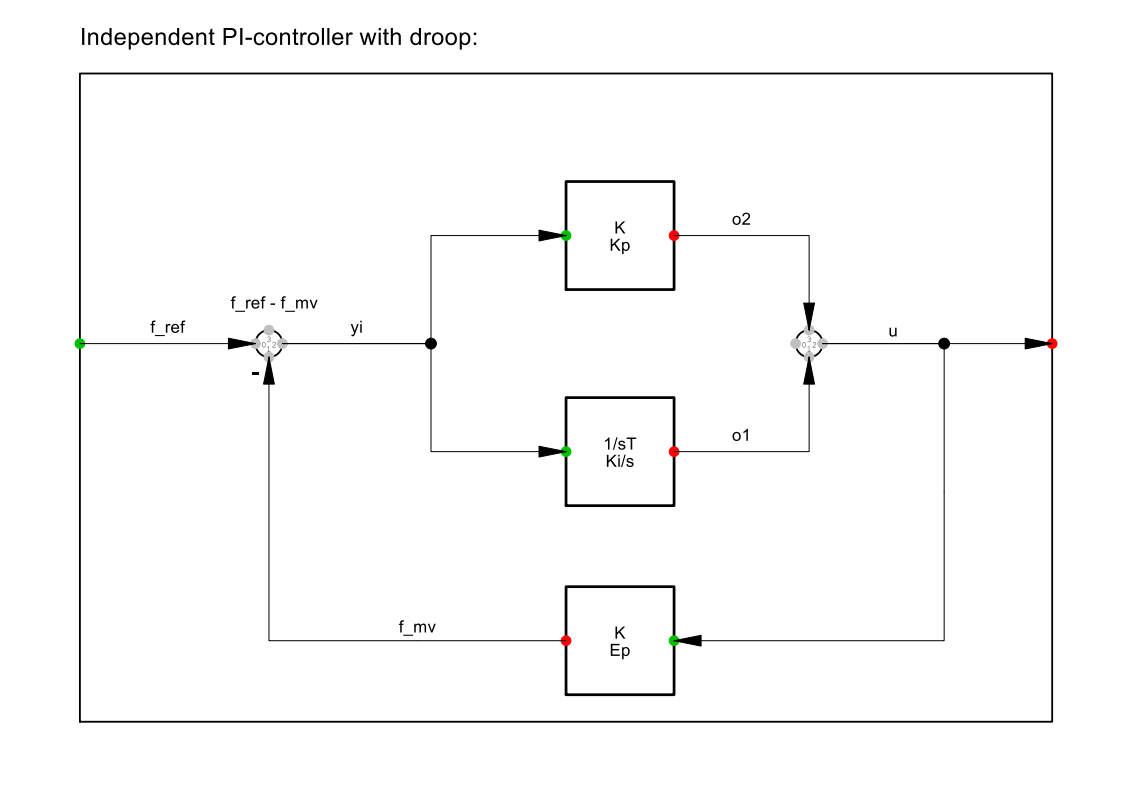


**Figure 11.** PI controller with droop (Nordic Analysis Group, 2023).

$T_{feedback}$ can be derived from equation

$$T_{feedback} = \frac{1}{K_i E_p}, \tag{26}$$

where $K_i$ is integral gain and $E_p$ is droop. The PI controller parameters can be scaled linearly with the droop so that the dynamic response scales with the static gain $1/e_p$. For the PI controller shown in Figure 11, this is achieved using the following equations

$$K = K_p e_p, \tag{27}$$

and

$$T = \frac{T_i}{e_p}, \tag{28}$$

where the parameters *T* and *K* are independent of the droop, and the droop parameter $e_p$ represents the regulating strength $E_p$ in per-unit value.

# 4 Simulation Model Development

The first task was to build a solid understanding of the technical documentation provided by ABB, especially the confidential internal materials related to hydropower plant control systems and simulation principles. Also, this included developing a solid understanding of the operation of a hydropower plant from the perspective of mathematical modeling. The documentation included block diagrams, test data, simulation results obtained from a test project, and parameter lists. It also described the key components relevant to this work, such as the Turbine Governor 800 (TG800).

The next step involved examining the technical requirements related to FCR provision by studying the standards established by the Nordic TSOs. ABB had also provided documentation describing the operation of the control system in a high-level block-diagram form, which supported the modeling work.

The second task consisted of building the simulation model in DIgSILENT PowerFactory software. The modeling process relied on ABB's internal documentation and on the technical requirements prepared by the Nordic TSOs. The purpose of this was to develop a simulation model which can represent the behavior of the hydropower plant and to examine how the Battery Energy Storage System (BESS) integrated into the simulation model affect the plant's power response during FCR provision.

The third task involved obtaining measurement data from a Finnish hydropower plant, which enabled the testing and validation of the simulation model by injecting field measurement data into the simulation model. In these tests, the results produced by the simulation model were compared with the actual behavior of the plant during frequency deviations in the grid. The tests focused primarily on power output, the response time of the modeled hydropower plant, and the quality of the produced power during a grid disturbance. Also, the influence of the energy storage system on the power output of

the hydropower plant and on the reduction of mechanical control movements was examined.

## 4.1 Different Models and their Validation Process

The simulation model developed in this thesis consisted of the turbine governor model, turbine model and an energy storage system model. Based on ABB's transfer function documentation (ABB, 2016), the focus of the modeling work was placed on the turbine governor module, which consists of the Speed Governor, Power Control, GV Reference and the GV and RB position loop and servomotor submodules. Also, the turbine model was developed using existing literature and prior studies on Kaplan turbine modeling.

To facilitate the modeling process, the simulation model was constructed module by module. Also, the excitation system and the energy storage system were implemented using DIgSILENT's pre-built template models in order to simplify the overall simulation structure and the validation process.

The validation process was initiated with the turbine model, after which the GV and RB Position Loop and Servomotor submodules were validated. Due to limitations in the available measurement data, the GV Reference and Speed Governor modules, as well as the Power Control module, had to be validated simultaneously. The energy storage system integrated into the simulation model could not be validated in this study, because no existing measurement data were available.

The measurement data included the GV and RB positions, the input frequency, the generator active power and hydraulic head of each measurement dataset. The sampling interval of the measurement data was 50 ms, and all modules were validated using the same measurement datasets for FCR-N, FCR-D up, and FCR-D down. Tests were conducted at different operating power levels.

### 4.1.1 Turbine

Based on the research articles examined in this study, a Kaplan turbine can be modeled in several different ways, many of which rely heavily on the availability of plant-specific input data. For example, the Kaplan turbine models presented in documents (Henrique Augusto Menarin et al., n.d.; Ruokolainen, 2016) are strongly based on measurement data from the turbine being modeled and include a wide range of static model parameters derived from index tests.

In building the turbine model, the nonlinear Kaplan model developed by Dmitri Kosterev (Kosterev, 2004) was utilized. Kosterev's model was selected because of its simplicity and because sufficient input data were not available for the other models. Another reason was that, when comparing Kundur's and Kosterev's nonlinear turbine models, Kosterev's model was found to be very similar to Kundur's model. The only difference between the two models is that Kundur's model is based on a single input signal, which is suitable, for example, for a Francis turbine. In Kosterev's model, the turbine input consists of two separate signals, which in turn was suitable for a Kaplan turbine. Kosterev's model is presented in Figure 12. Due to confidentiality obligations, the parameter values in Table 6 are not discussed in further detail.

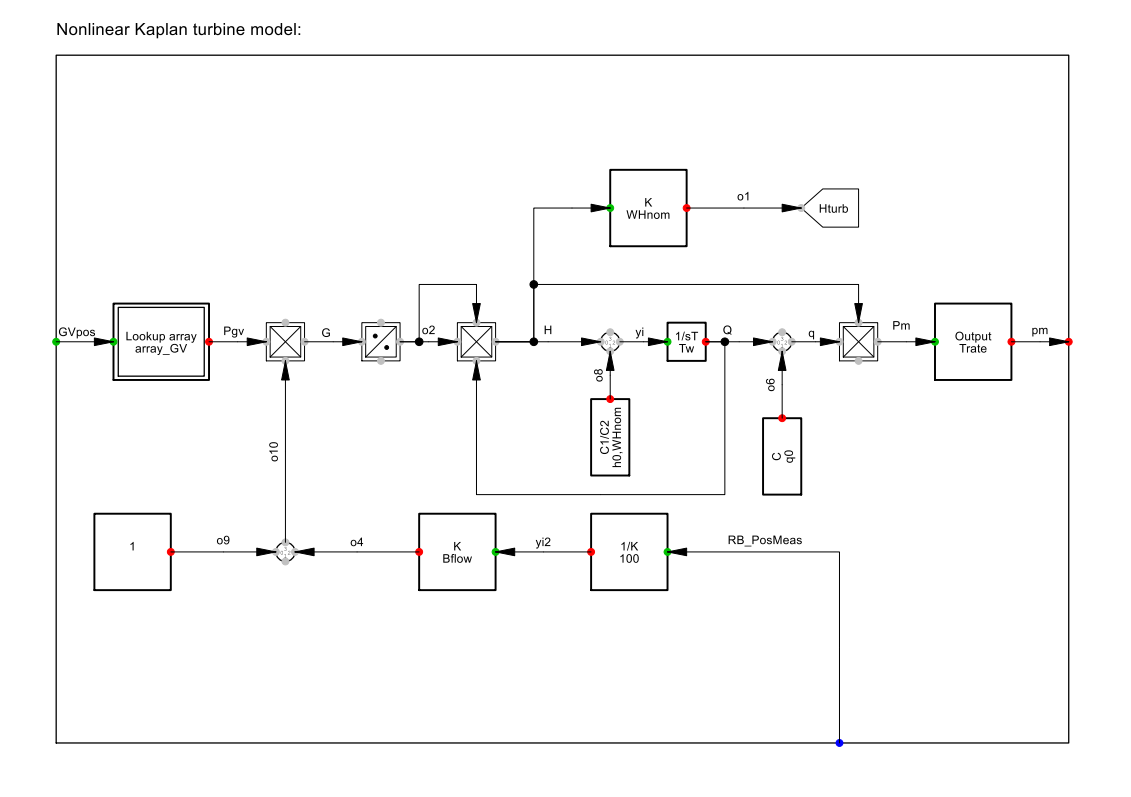


**Figure 12.** Nonlinear Kaplan turbine model based on Kosterev's model.

**Table 6.** Turbine parameters.

| Parameter | Description | Unit |
|---|---|---|
| $T_w$ | Water time constant | s |
| $h_0$ | Steady-state head | m |
| $q_0$ | No-load turbine flow | pu/pu |
| $B_{flow}$ | Gain representing blade angle impact on the turbine water flow | pu/pu |

The turbine validation was carried out using site measurement data, which had been performed at different power levels during site measurement tests with a sampling interval of 50 ms. Validation was performed using FCR-N sine-wave tests, FCR-N step-sequence tests, and FCR-D Down and Up fast-ramp tests. The GV and RB position values obtained from the measurement data were directly applied as inputs to the turbine

model. Later, RMS simulations were performed, in which the power output produced by the simulation model was compared with the real measured power data.

To account for the dependence of turbine power on the combined positions of the GV and RB, a nonlinear relationship between the *GVpos* and the partial turbine power contribution *Pgv* was modeled using the lookup table array GV shown in Figure 12. The purpose of this lookup table is to represent off-cam operating conditions by describing how turbine power grows when the GV position increases without a corresponding increase in RB position. In practice, a Kaplan turbine can temporarily operate in an off-cam condition during dynamic operation, when the GV position changes before the RB position has adjusted accordingly.

In Figure 12, when *RB PosMeas* is zero, the turbine power contribution is proportional to *Pgv* only, resulting in strong power saturation even with increasing GV position, as water flow cannot increase optimally with the RB closed. When the RB position increases together with the GV position, a gain greater than one is applied to *Pgv*. This allows the turbine power to continue increasing. Therefore, the array GV represents the nonlinear behavior between GV and RB when their positions are not on the optimal combination curve. These off-cam situations are mainly caused by mechanical delays.

According to (Zhao et al., 2015), the turbine control signal *G* shown in Figure 12, can be defined with formula

$$G = f(y) \cdot f(y_r), \tag{29}$$

where *f(y)* is GV position and $f(y_r)$ is RB position. The function *f(y)* can be expressed as fifth-order polynomial equation

$$f(y) = b_5 y^5 + b_4 y^4 + b_3 y^3 + b_2 y^2 + b_1 y + b_0, \tag{30}$$

where $b_5$, $b_4$, $b_3$, $b_2$, $b_1$ and $b_0$ are the constant polynomial coefficients. RB position $f(y_r)$ is defined linearly with equation

$$f(y_r) = y_r \cdot B_{flow} + 1, \tag{31}$$

where $B_{flow}$ demonstrates the coefficient which determines how blade angle influences the turbine's water flow.

In order to determine the coefficients associated with the GV and RB positions, it was also necessary to account for the plant-specific hydraulic head and steady-state head. This was accomplished by collecting measurement data from the hydropower plant, considered in this study at as many different operating power levels as possible. From the dataset, the power output, GV position, RB position, and hydraulic head were recorded.

Based on the collected data, the coefficients $b_5$, $b_4$, $b_3$, $b_2$, $b_1$, $b_0$ and $B_{flow}$ of the lookup table array GV were optimized using Python's SciPy minimize function by minimizing the sum of squared errors between the measured turbine power and the calculated turbine power. The turbine power was computed for each data point using the corresponding steady-state hydraulic head. The use of the linearization table array GV made it possible to neglect the no-load turbine flow parameter $q_0$. Figure 13 present fifth order fitting curve in lookup table array GV.

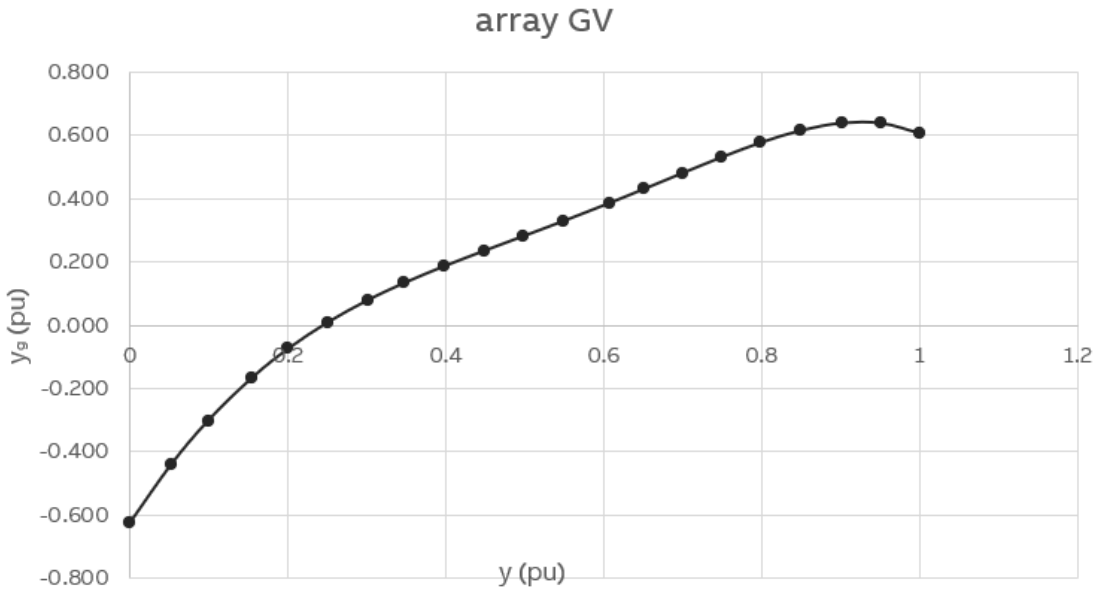


**Figure 13.** Fifth order fitting curve in array GV.

The following plots illustrate simulated responses obtained from the turbine RMS simulations. Other simulation cases are not presented in this thesis due to confidentiality obligations.

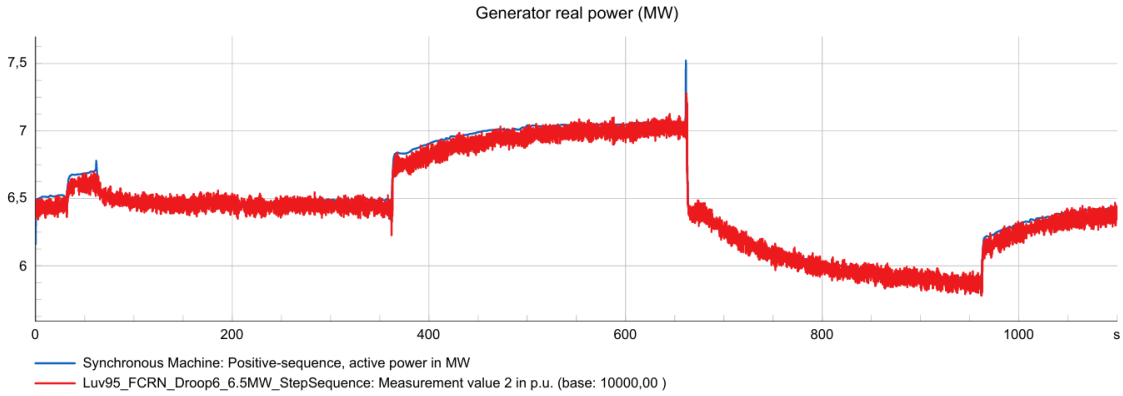


**Figure 14.** FCR-N step sequence test: generator real power (MW), measured data (red) and simulated response (blue).

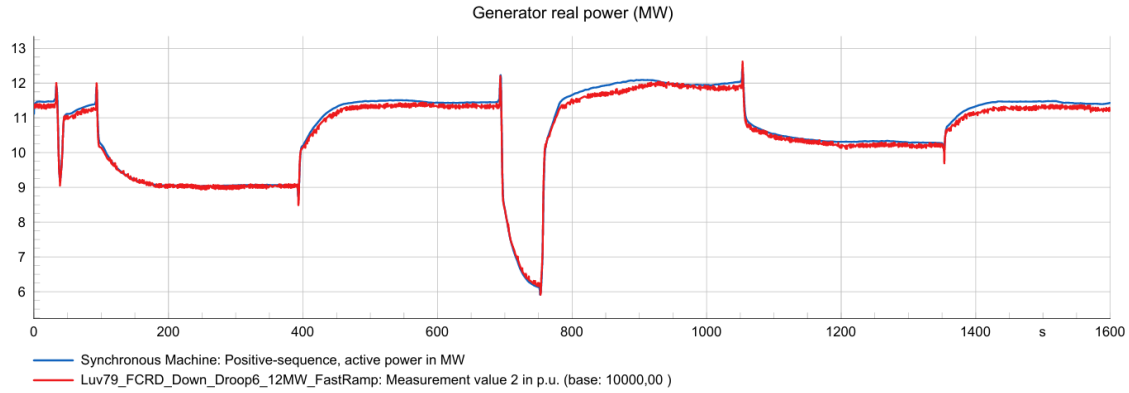


**Figure 15.** FCR-D Down fast ramp test: generator real power (MW), measured data (red) and simulated response (blue).

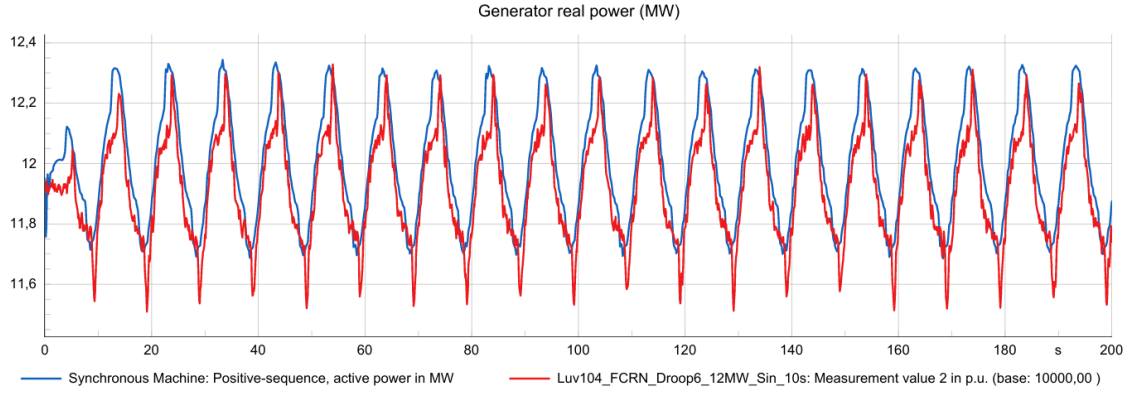


**Figure 16.** FCR-N sine test 10 seconds: generator real power (MW), measured data (red) and simulated response (blue).

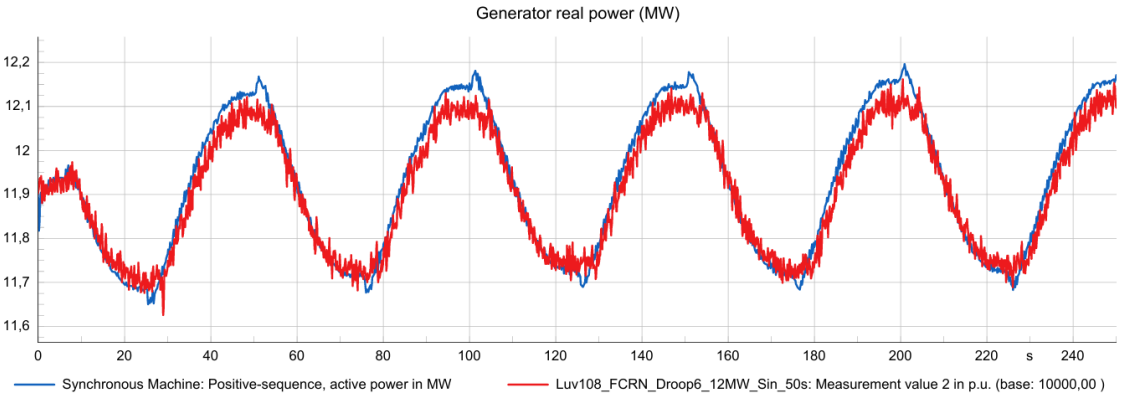


**Figure 17.** FCR-N sine test 50 seconds: generator real power (MW), measured data (red) and simulated response (blue).

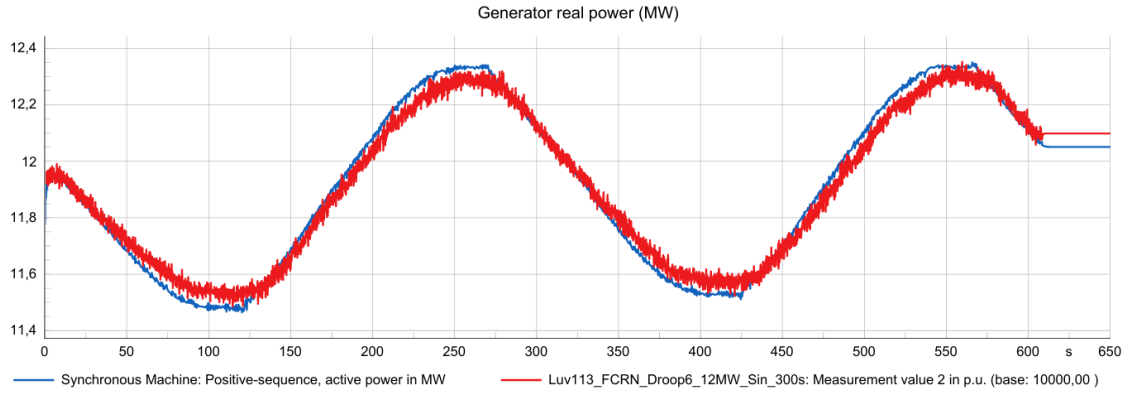


**Figure 18.** FCR-N sine test 300 seconds: generator real power (MW), measured data (red) and simulated response (blue).

### 4.1.2 Turbine Governor TG800

The turbine governor TG800 was modeled in accordance with ABB Document (ABB, 2016b). The validation of the governor was carried out in stages where the measured GV and RB positions were compared with the simulated positions by applying the measured test frequency to the GV Reference and Speed Governor module. The validation process was significantly complicated by the interdependencies between the Power Control, GV Reference and Speed Governor, and GV Position Loop and Servomotor submodules. Energy storage and Frequency Control modeling will be carried out in next section.

In the TG800 governor, the RB position is calculated directly from the GV position. Therefore, from a validation perspective, it was most appropriate to begin with the validation from the GV position. The validation process was initiated by parameterizing the model with the data of the hydropower plant under study, including the FCR control parameters and control logic, mechanical time constants, nominal power, scaling factors of the lookup tables, and any applicable control functions. Figure 19 presents the model overview of the TG800 governor, illustrating the internal signal interconnections between the modules.

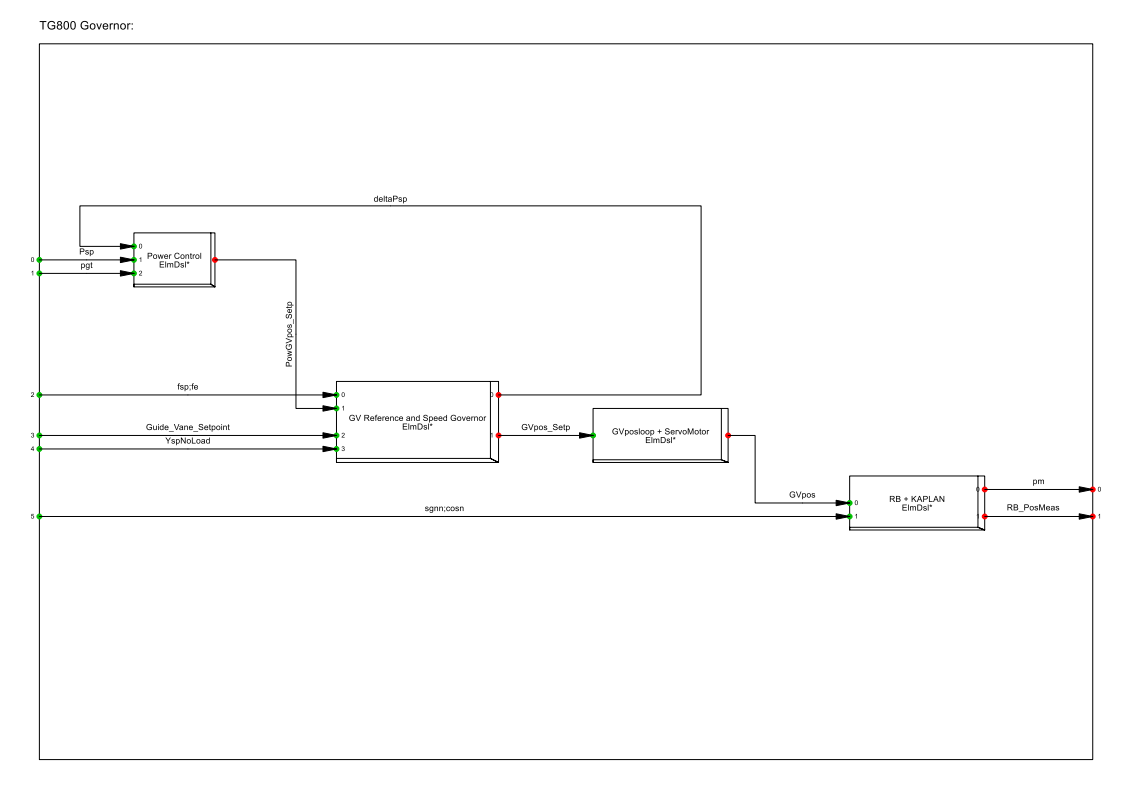


**Figure 19.** TG800 model overview.

The calculation of the GV position was performed within the GV Reference and Speed Governor, Power Control and the GV Positioning Loop and Servomotor modules. During the validation of the GV position, the RB position was taken directly from the measurement data, ensuring that the simulated turbine power remained sufficiently close to the measured power for validation purposes. Frequency test signal was fed as described in document (ABB, 2016b), the GV Reference and Speed Governor module receives the frequency reference value, the generator frequency, and the GV position setpoint calculated in the Power Control module. Based on these inputs, the GV position signal is computed and passed to the GV Positioning Loop and Servomotor module. The FCR control blocks presented in document (ABB, 2016b) were implemented within the GV Reference and Speed Governor module to enable the simulation of different FCR products. The FCR Speed Droop blocks were modeled in accordance with ENTSO-E document (Gierling, 2025), and implemented for FCR-N, FCR-D up, FCR-D down, FSM, LFSM-O, and LFSM-U control modes.

In the Power Control module, the generator active power, power reference, and the FCR control signal received from the GV Reference and Speed Governor are used to produce the GV position setpoint that is sent back to the GV Reference and Speed Governor module. In contrast to document (ABB, 2016b), the modeling was implemented only using a feedforward table, consistent with the implementation applied in the hydropower plant used for validation. The GV position setpoint calculated in the Power Control module also considers the ratio between the steady-state head and the nominal head, which must correspond to the values used in the turbine model.

The GV Position Loop and Servomotor submodule represents the mechanical inertia, backlash, and hydraulic characteristics of the GV mechanism. The parameters describing these effects were determined by comparing the simulated GV position going to the turbine with the measured GV position. The following Figures present a subset of the GV position responses. The remaining responses have been left out from this thesis due to confidentiality obligations. The simulated GV position is shown in blue and the measured position in red.

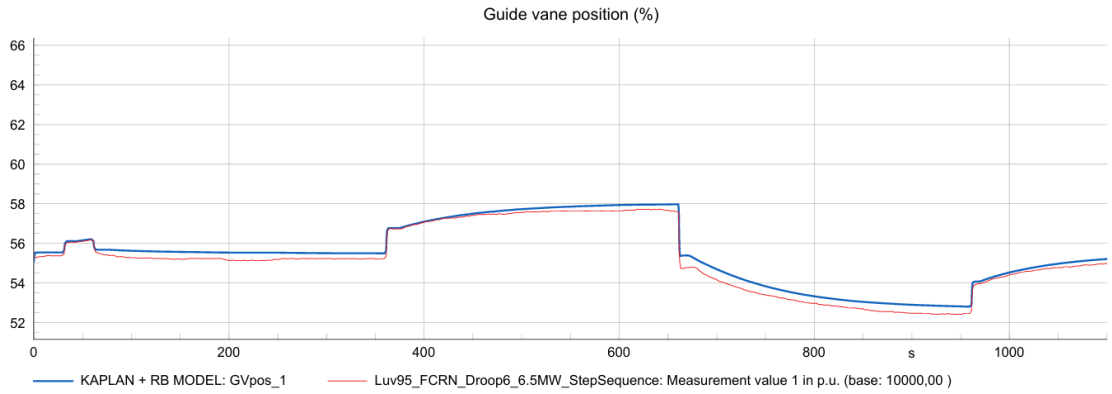


**Figure 20.** FCR-N step sequence test: guide vane position (%), measured data (red) and simulated response (blue).

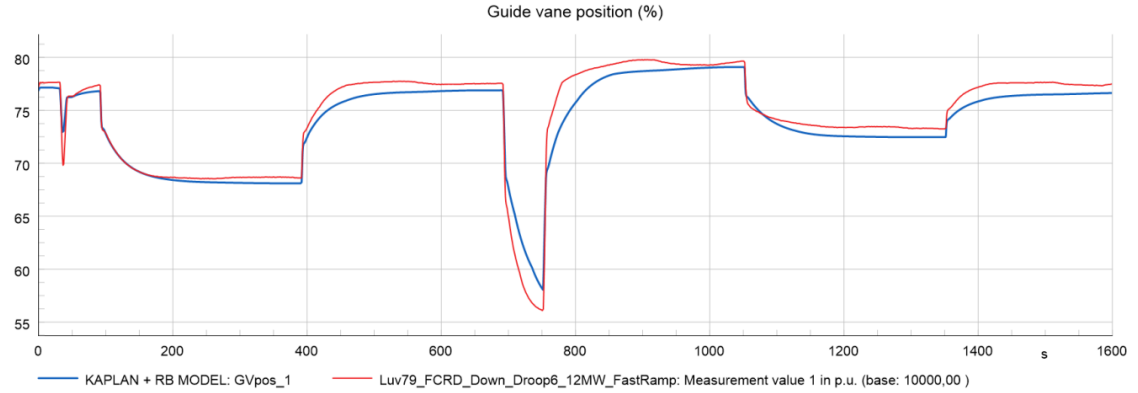


**Figure 21.** FCR-D Down fast ramp test: guide vane position (%), measured data (red) and simulated response (blue).

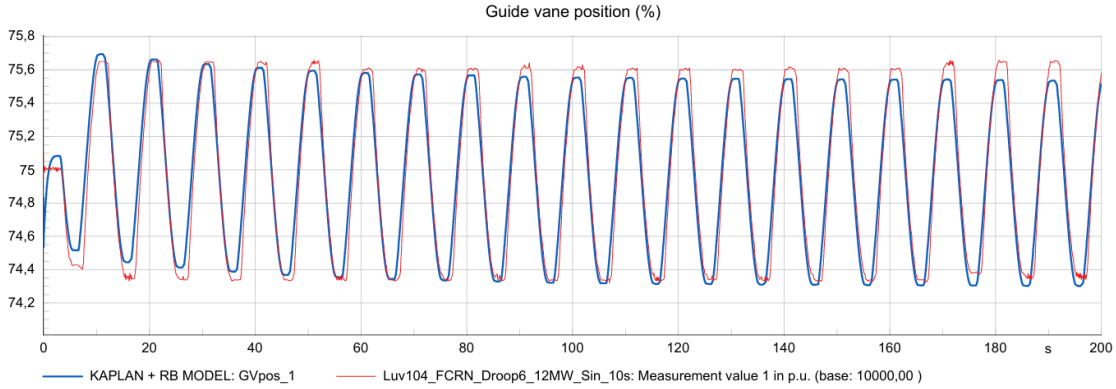


**Figure 22.** FCR-N sine test 10 seconds: guide vane position (%), measured data (red) and simulated response (blue).

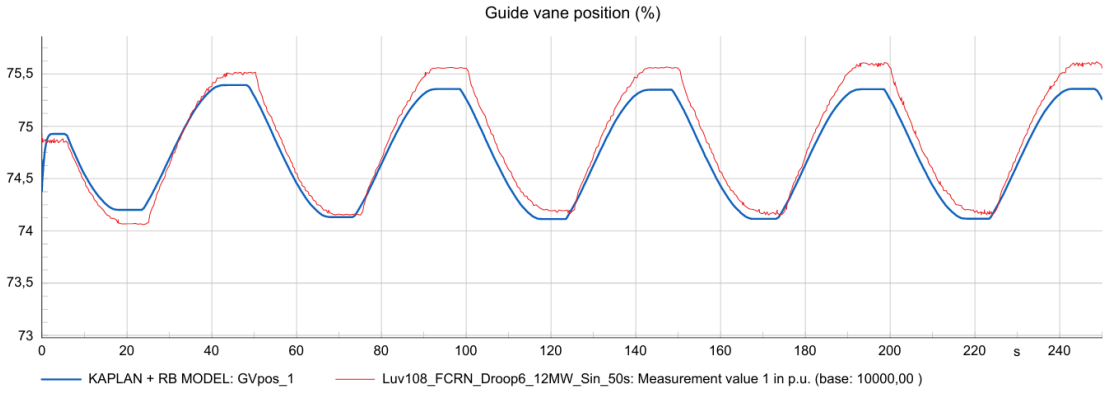


**Figure 23.** FCR-N sine test 50 seconds: guide vane position (%), measured data (red) and simulated response (blue).

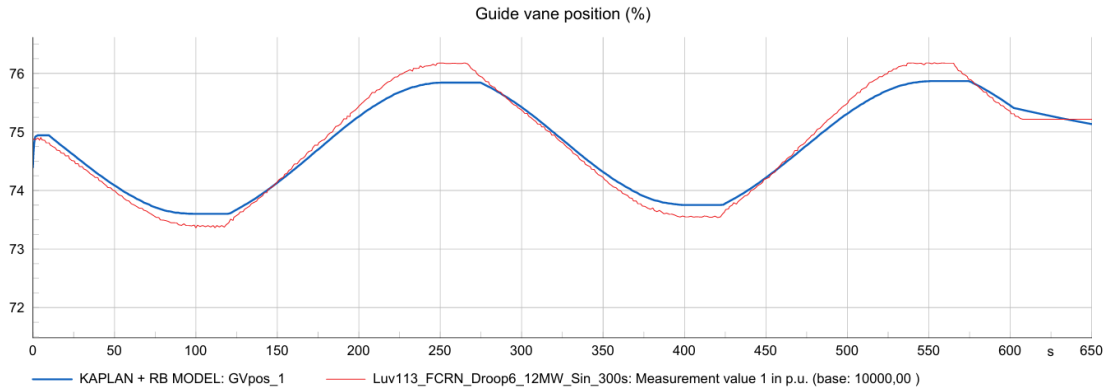


**Figure 24.** FCR-N sine test 300 seconds: guide vane position (%), measured data (red) and simulated response (blue).

As previously mentioned, the RB position is calculated from the GV position supplied to the turbine model. In contrast to document (ABB, 2016b), the computational determination of the upstream and downstream water levels used for defining the RB position setpoint value has been replaced with a steady-state head parameter value in RB Reference module. This modification was implemented due to the developed turbine model and for the sake of simplicity. The combination curve used to determine the RB position setpoint, together with the GV and RB linearization tables, includes the same steady-state head parameter as the turbine model, ensuring that the calculation is performed correctly for each operating condition. Modifications were also made to the RB reference module by removing the RB Governor PI controller presented in ABB's documentation (ABB, 2016b). As a result of this change, the RB position setpoint signal is generated in the simulation model using a feedforward gain and a feedforward lookup table.

The mechanical inertia and hydraulic characteristics of the RB position were modeled by feeding the obtained RB position setpoint to the RB Position Loop and Servomotor submodule, which was implemented within the same module as the Kaplan turbine model.

The RB position validation was conducted by using the measured GV position as an input, so that the initial data for the RB position validation were as accurate as possible. The following Figures illustrate simulated RB responses obtained from the RMS simulations.

Other simulation cases are not presented in this thesis due to confidentiality obligations. The simulated RB position signal supplied to the turbine is shown in blue and the measured RB position in red.

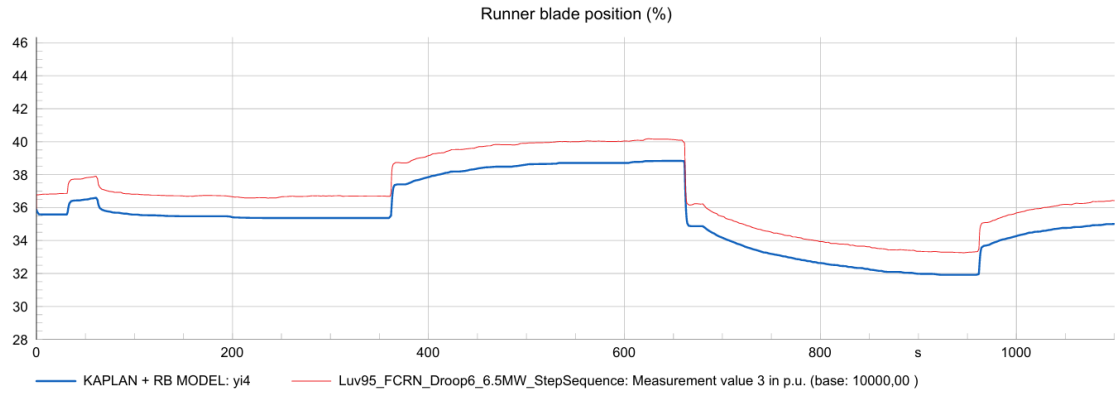


**Figure 25.** FCR-N step sequence test: runner blade position (%), measured data (red) and simulated response (blue).

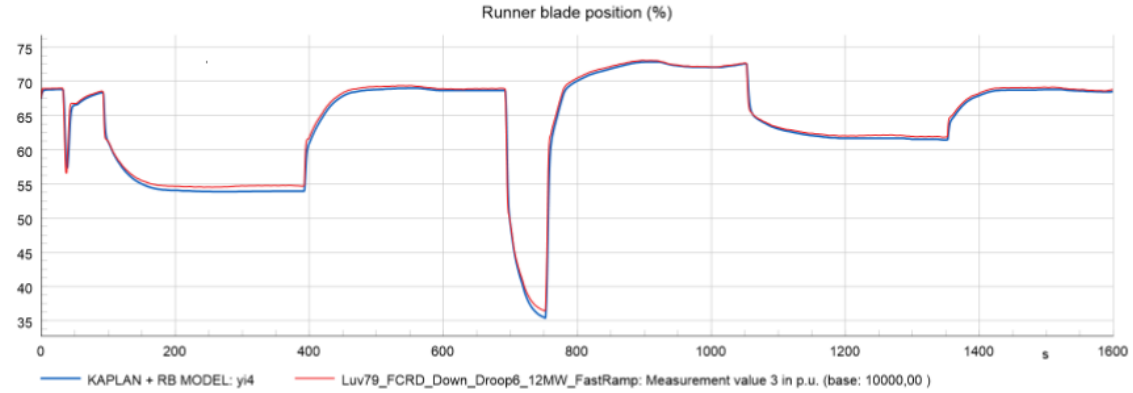


**Figure 26.** FCR-D Down fast ramp test: runner blade position (%), measured data (red) and simulated response (blue).

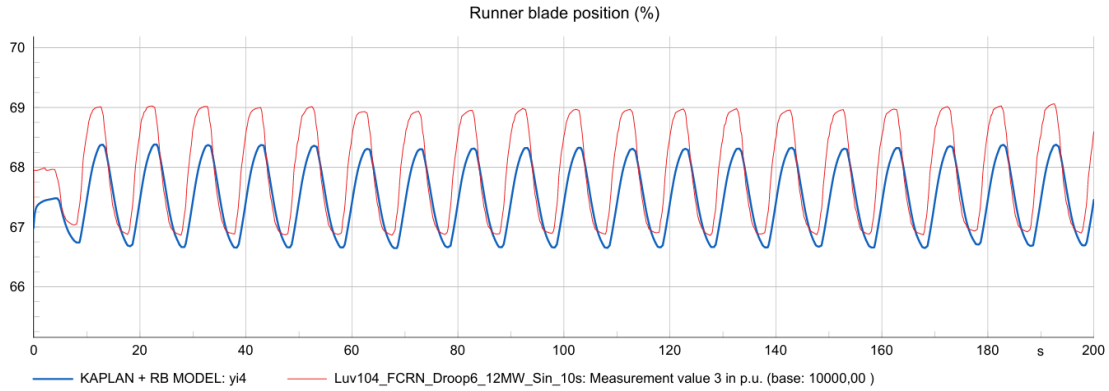


**Figure 27.** FCR-N sine test 10 seconds: runner blade position (%), measured data (red) and simulated response (blue).


**Figure 28.** FCR-N sine test 50 seconds: runner blade position (%), measured data (red) and simulated response (blue).


**Figure 29.** FCR-N sine test 300 seconds: runner blade position (%), measured data (red) and simulated response (blue).

### 4.1.3 Complete Model Validation Process

After the GV position and RB position had been validated, the turbine governor and turbine model were validated as a complete system. During the validation, the external signals for the GV and RB positions were disconnected, and the measured frequency signal was applied to the GV Reference and Speed Governor module. For the validation, the turbine governor was configured with the same parameter settings that had been used in the corresponding measurement data test, and these settings were obtained from the TG800 governor information and documentation used in the site measurement tests. The parameters placed to the turbine model during the turbine validation remained unchanged for all tests. The following Figures illustrate simulated responses obtained from the complete model RMS simulations. Other simulation cases are not presented in this thesis due to confidentiality obligations. The simulated signals are shown in blue, the measured signals are shown in red, and the input frequency signal is shown in orange.

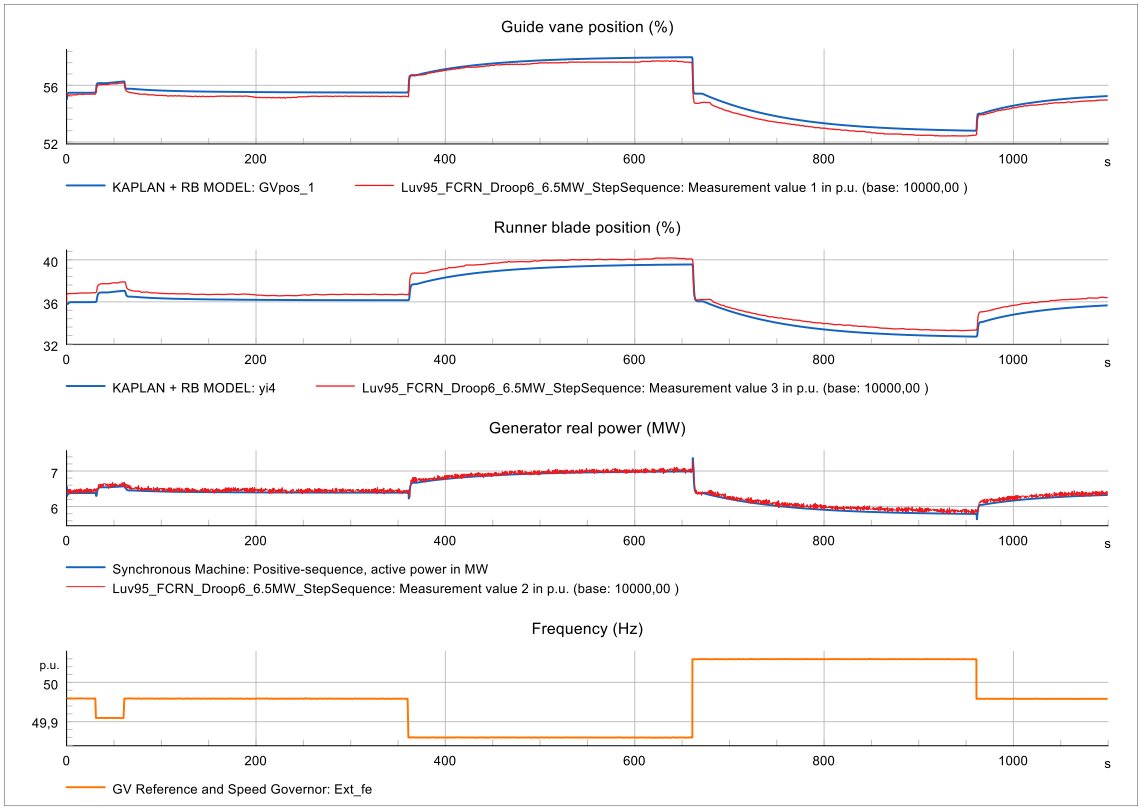


**Figure 30.** FCR-N step sequence test: measured data (red) and simulated response (blue).

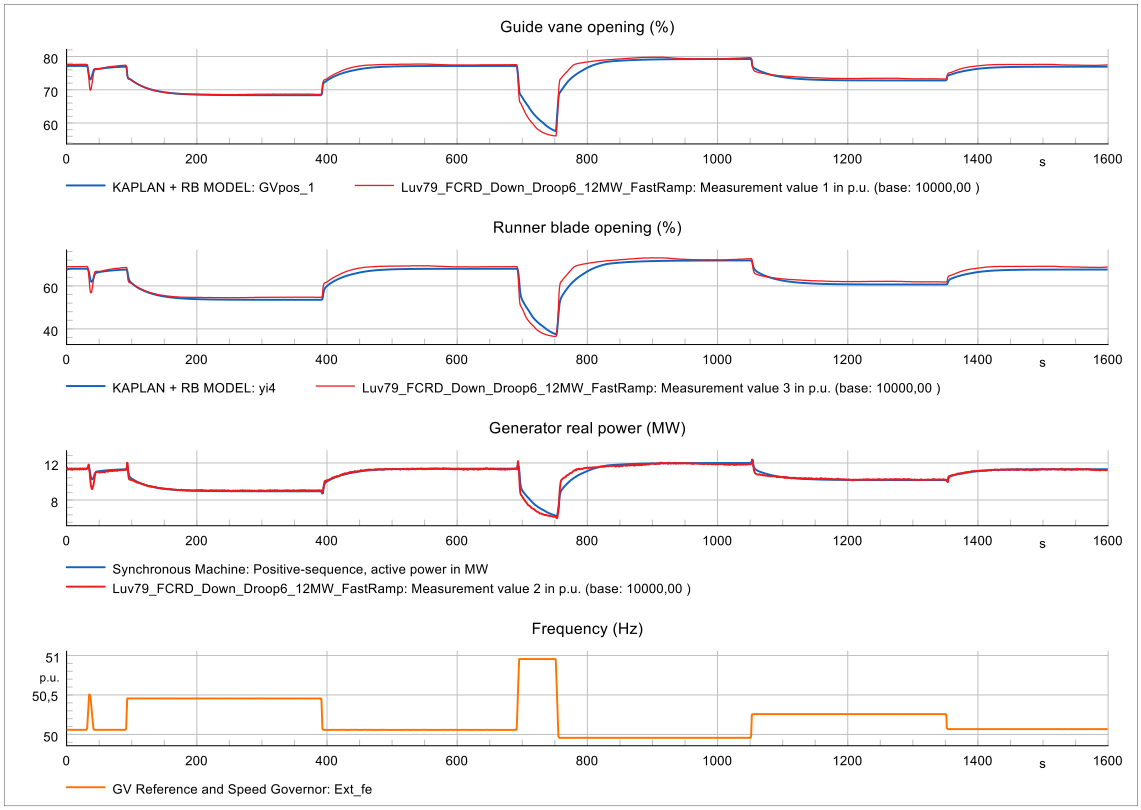


**Figure 31.** FCR-D Down fast ramp test: measured data (red) and simulated response (blue).

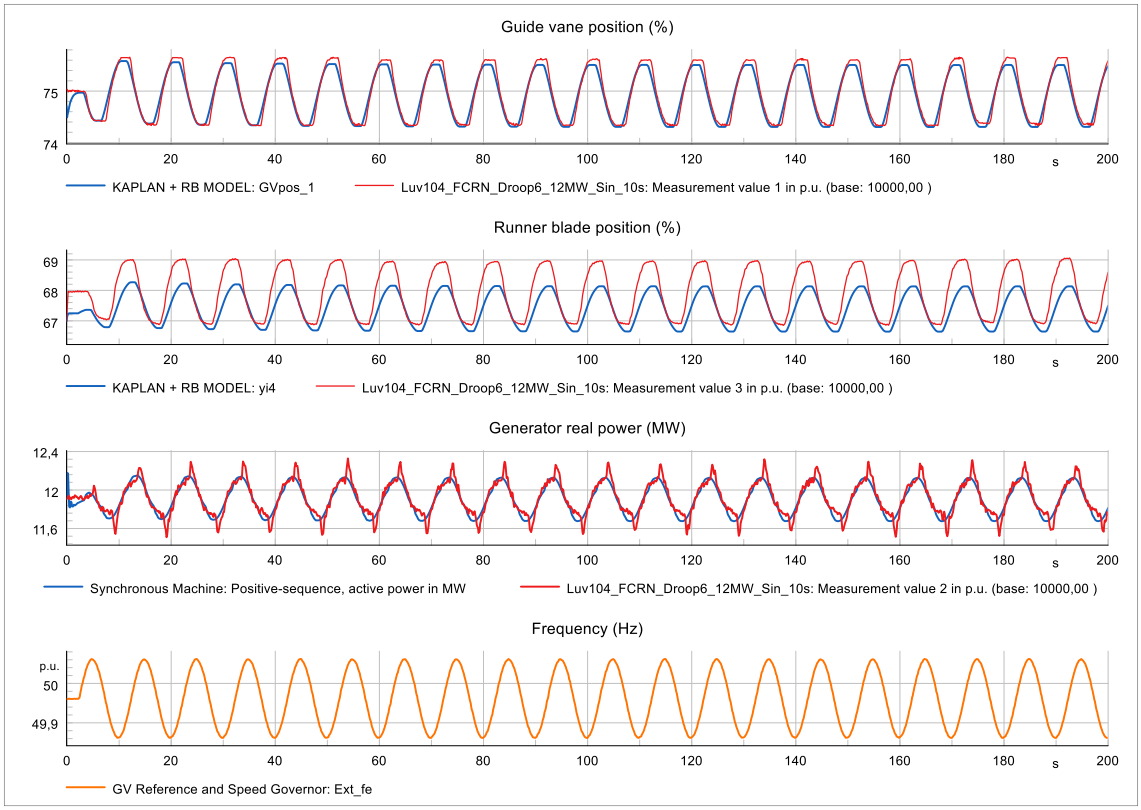


**Figure 32.** FCR-N sine test 10 seconds: measured data (red) and simulated response (blue).

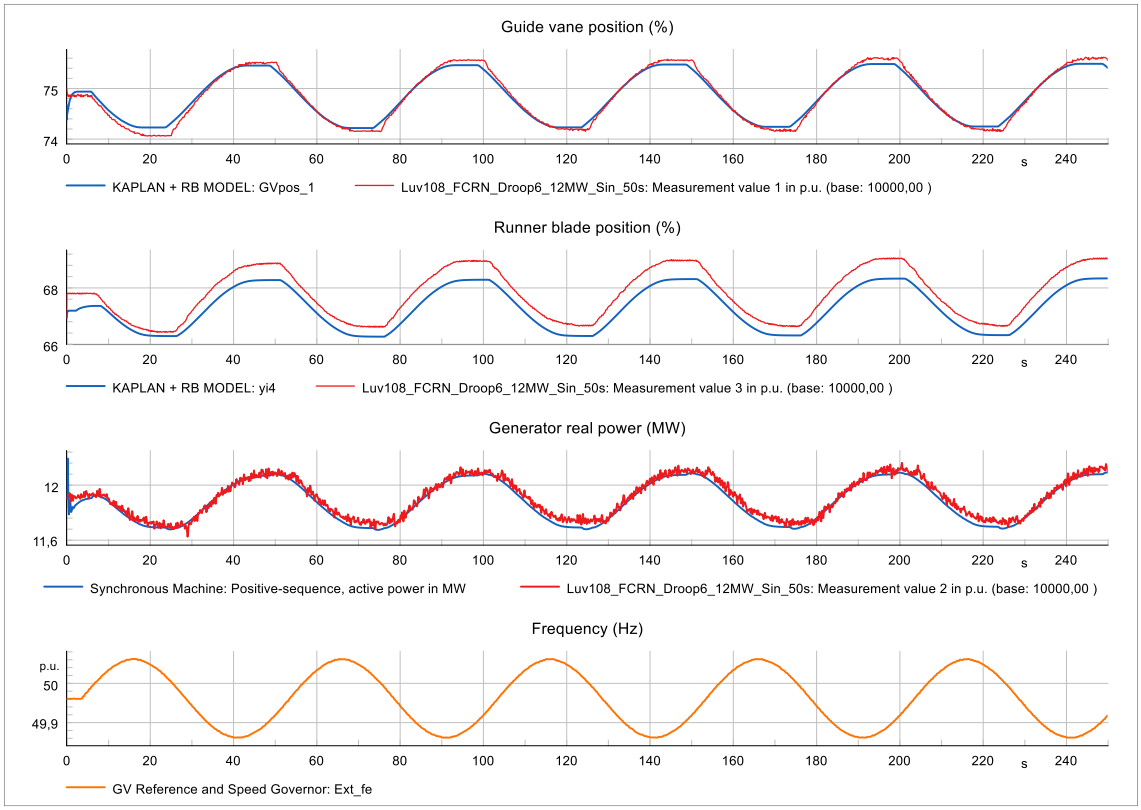


**Figure 33.** FCR-N sine test 50 seconds: measured data (red) and simulated response (blue).

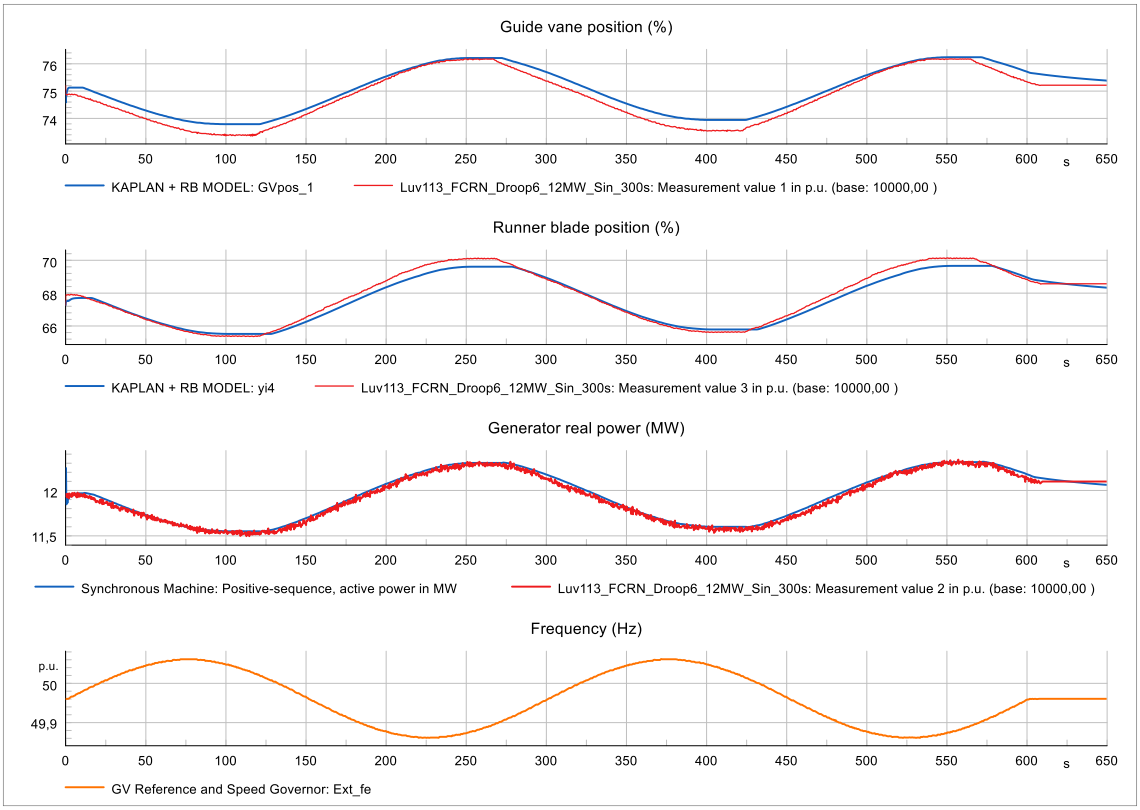


**Figure 34.** FCR-N sine test 300 seconds: measured data (red) and simulated response (blue).

## 4.2 Integration of Energy Storage and Frequency Control

In terms of the energy storage system and its frequency control, it was decided to use DIgSILENT's pre-built template, "DIgSILENT BESS FrequencyCtrl 10 kV 30 MVA,". The reason for this was that the primary objective of this study was to investigate the power output of the energy storage system and its influence on hydropower plant performance in frequency support, and how it could be used to reduce fine adjustments of the GV and RB positions during continuous frequency control. This decision was further supported by Gonzalez-Longatt (Gonzalez-Longatt & Rueda Torres, 2021), which also provided insight into the modeling of converter-dominated power systems, including the operation and behavior of energy storage systems in dynamic simulations. The template is a generic model that includes a battery and a grid-side converter, and it is implemented in DIgSILENT Simulation Language (DSL). The Battery Energy Storage System (BESS) has

an apparent power rating of 30 MVA and a connection voltage of 10 kV. The model is suitable for dynamic RMS simulations (DIgSILENT GmbH, 2025).

The battery model was integrated with the TG800 turbine governor in accordance with document (ABB, 2016a) by taking the control signal for the hybrid controller directly from the turbine governor's Power Control module, also the Frequency Control of the pre-built BESS model was replaced by the frequency control implemented within the turbine governor. Figure 35 presents an overview of the modified BESS model integrated with the turbine governor, where the *dpref* signal represents the signal received from the hybrid controller.

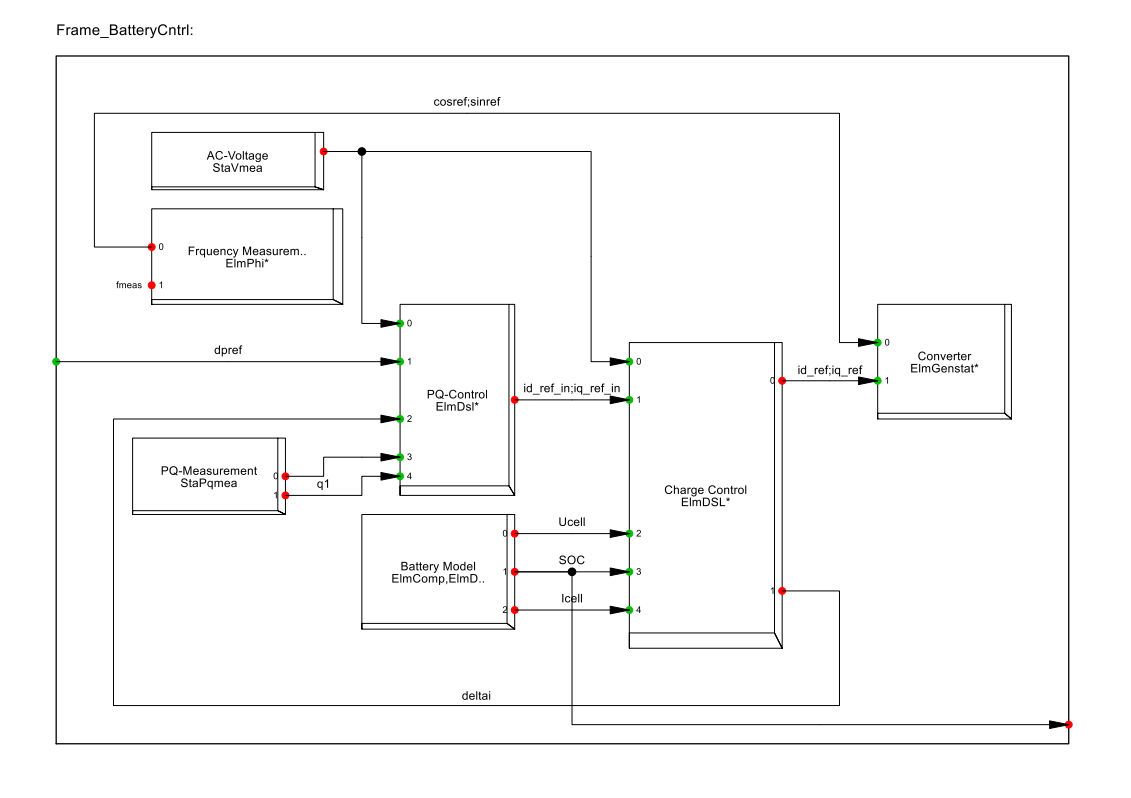


**Figure 35.** Modified BESS control frame.

The battery model's State of Charge (SOC) control was modified to make it compatible with the turbine governor connections. The SOC signal was taken as a separate output from the Battery Model, as shown in the lower right corner of Figure 35. SOC was

excluded from the analysis, as well as a techno-economic analysis regarding the sizing of the BESS system. The battery size and power rating of the battery model were adjusted to make them more suitable for FCR control in a hydropower plant by modifying the Simple Battery module parameters of the battery model.

In the following sections, the influence of the energy storage system on the hydropower plant's power output, GV and RB movements, and overall performance was tested by simulating FCR tests and by using historical frequency data obtained from Fingrid's website (*Frequency - Historical Data*, n.d.). Historical data were used to analyze GV and RB movements, whereas the FCR tests were used to investigate power output and performance with FCP-IT simulation tool provided by Fingrid.

### 4.2.1 FCR Requirement Tests

The influence of the energy storage power output on the hydropower plant's power response was investigated by running simulations using the FCR-N sine and step-sequence tests with hybrid governor system. The tests examined how the extra power produced by the energy storage system affects the plant's stability and overall power output compared to site measurements. The results obtained from the simulation model were fed into Fingrid's simulation FCP-IT tool, which was used to assess compliance with the FCR requirements in FCR-N provision.

Figure 36 presents the BESS output during a 0.1 Hz frequency change. In the tests, the active power produced by the BESS system was set to 0.26 MW/0.1 Hz, which means that 0.26 MW of power is delivered when the frequency changes by 0.1 Hz. At the same time, the hydropower plant's total FCR-N capacity was 0.6 MW/0.1 Hz.

Figure 36 shows that the BESS output decreases before the applied step response begins to return to the steady-state value. The purpose of the BESS is to support power

production during the periods when the turbine itself, due to its inherent inertia, is unable to reach the power reference quickly enough.

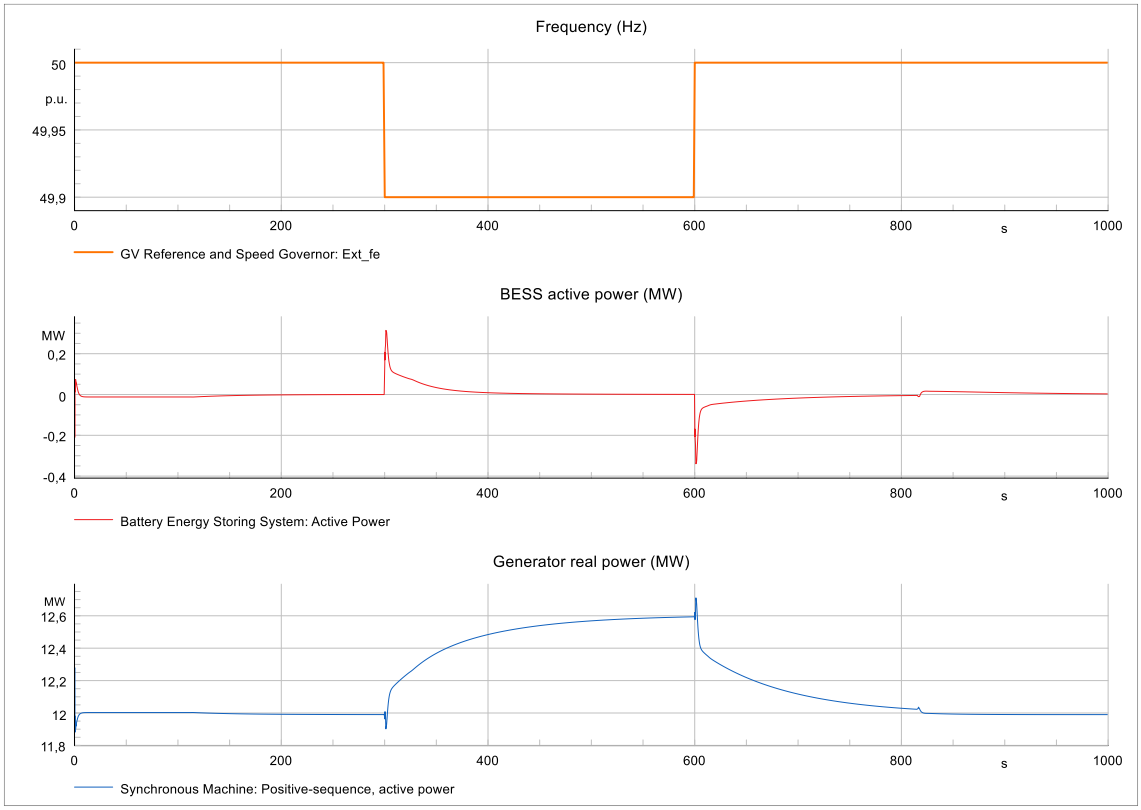


**Figure 36.** BESS power output.

The simulated model equipped with the hybrid controller and the site measurement data obtained from the hydropower plant were fed into the FCP-IT tool to evaluate the stability requirements. Stability was assessed using the Nyquist stability criterion. Figure 37 presents the Nyquist curves, where the hybrid model is shown on left and the measurement data without the hybrid model is shown on the right.

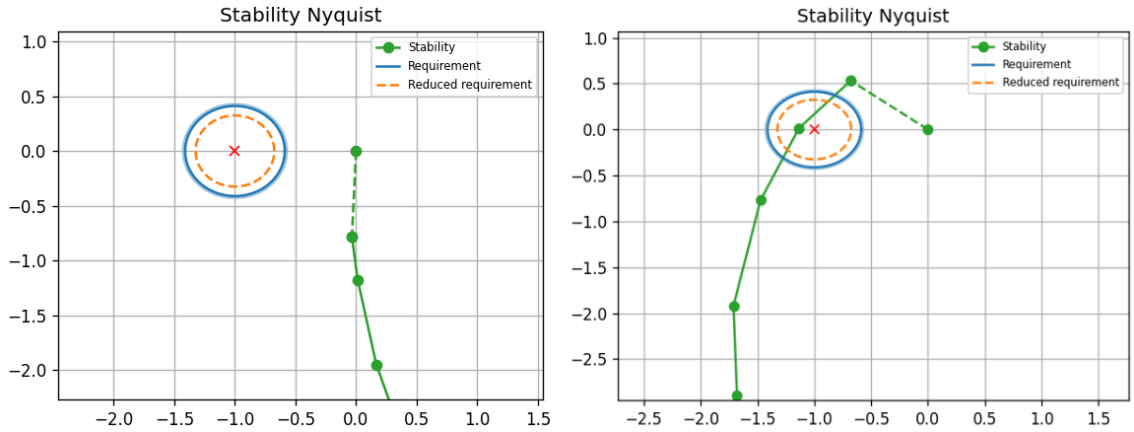


**Figure 37.** Stability Nyquist criterion curves for hybrid (left) and non-hybrid (right) models.

As mentioned in Section 2.4.4, for the system to be stable, the Nyquist curve must pass to the right of the point (−1, 0*j*) and it cannot cross over the circle in that area. Further information on system stability is provided in sources (Åström & Murray, 2021; Valtonen & Lehtovuori, 2017).

Stability was also assessed using the FCP-IT tool's FCR circles where, according to ABB's previous studies, the 10 second and 15 second tests had proven challenging with respect to the requirements. Figure 38 presents the 10 second and 15 second FCR circles, with the data for the system equipped with the hybrid controller shown on the left and the measurement data without the hybrid controller shown on the right.

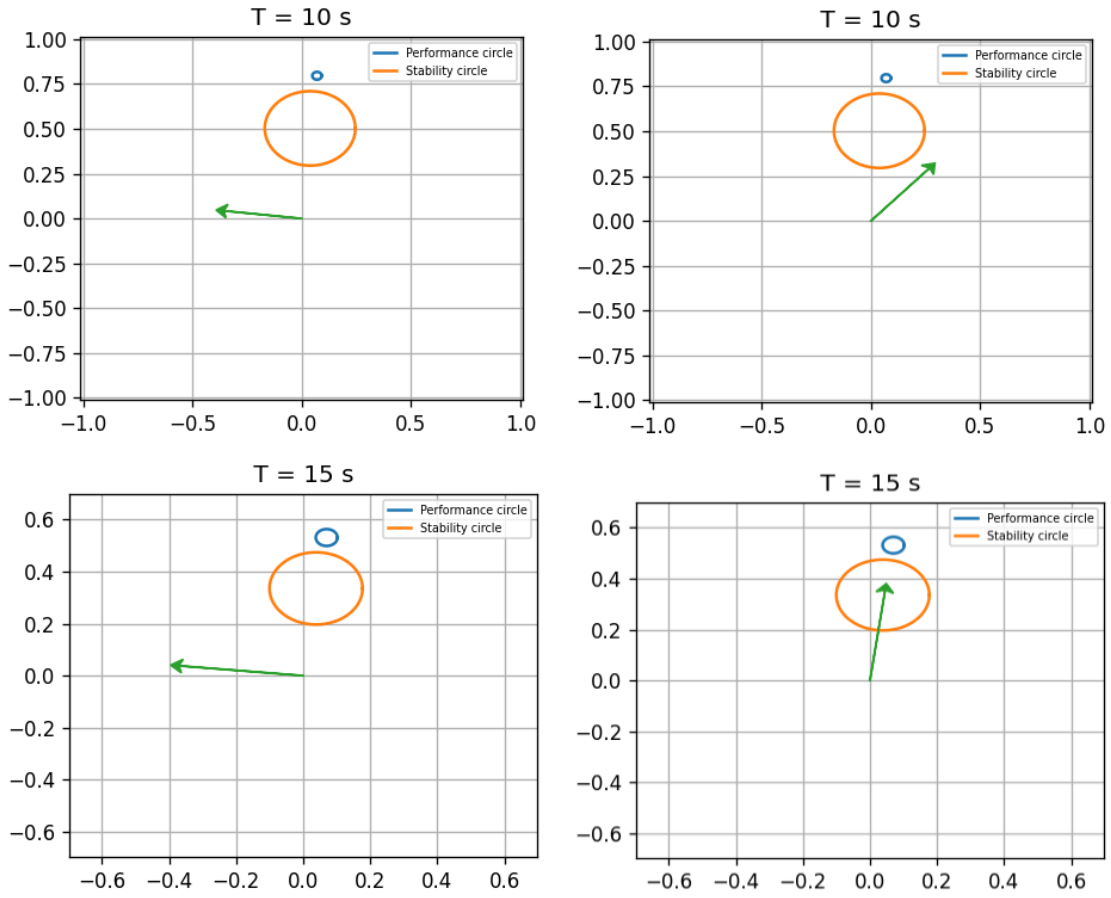


**Figure 38.** FCR circles for hybrid (left) and non-hybrid (right) models.

In the FCR circles shown in Figure 38, the performance and stability circles present pre-defined limit values. The stability requirement is fulfilled if the vector in the Figure 38 points to the left and does not enter into the stability circle (Kuivaniemi et al., n.d.).

The FCR-N performance criteria were evaluated in the FCP-IT tool using simulated Bode plots. The data from the simulation model equipped with the hybrid controller and the measurement data were fed into the FCP-IT tool in the same manner as in the stability evaluation. Figure 39 presents the Bode plots for the system equipped with the hybrid controller and for the measurement data without the hybrid control system. The hybrid controller plot is shown on the left, and the measurement data plot is shown on the right.

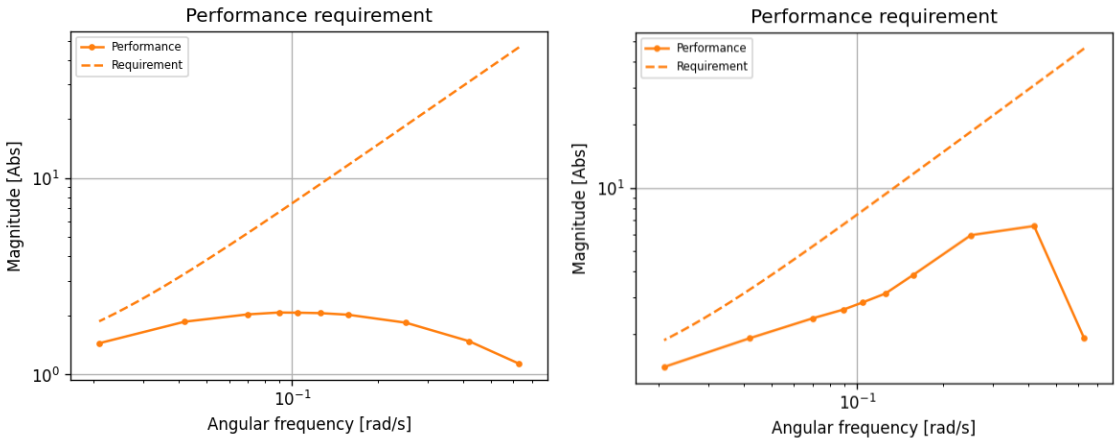


**Figure 39.** Performance criterion curves with all angular frequencies for hybrid (left) and non-hybrid (right) models.

The performance criterion is fulfilled if the measured performance curve stays below the performance requirement curve. Further information on the performance criterion is provided in source (Kuivaniemi et al., n.d.). Figure 39 presents the simulated performance criterion from all tests. In the model equipped with hybrid control on the left, the performance criterion remains significantly lower than in the model on the right, where no hybrid controller was used. However, the results may still vary, particularly in tests with higher angular frequencies and faster frequency periods, in which case the performance criterion of the hydropower unit may produce poorer results.

### 4.2.2 GV and RB Movements

The purpose of the integrated energy storage system is to improve the performance of hydropower plants with slow dynamics, while also reducing the wear and tear on the GV and RB caused by regulation. This section presents how the integrated BESS reduces GV and RB movements in a plant providing the FCR-N reserve.

The movements were investigated by simulating historical frequency data obtained from Fingrid's website and applying it to the simulation model's Alternating Current (AC) voltage source shown in single line diagram in Figure 40. In this case AC voltage source

represents external grid. The simulation results were compared by computing the sum of absolute differences between consecutive samples, corresponding to the discrete total variation of the signal (Tibshirani, 2022), which was implemented with Python. This enabled the reduction in movements to be calculated. The movements were also simulated in PowerFactory, which allowed plots of the frequency and the GV and RB movements to be generated.

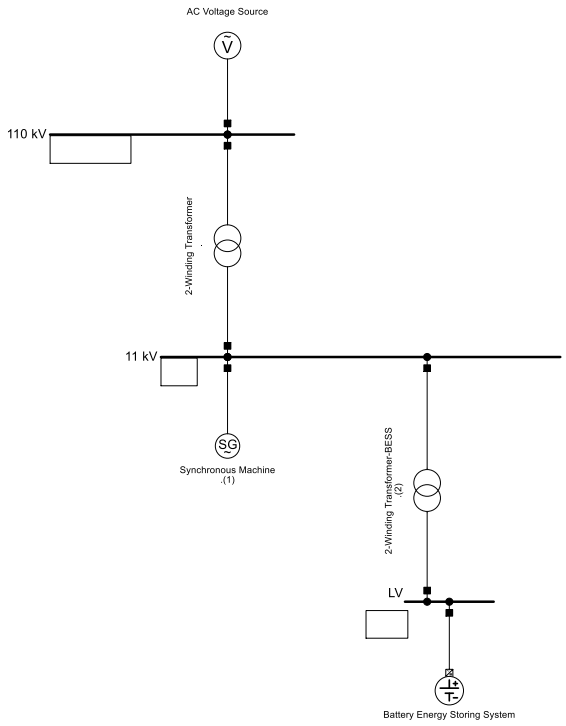


**Figure 40.** Single line diagram.

To reduce GV and RB movements, the power produced by the BESS had to be considered in the turbine control, such that the turbine and the BESS operated within predefined limit values. With a BESS active-power setting of 0.26 MW/0.1 Hz, the turbine control was disabled for frequency deviations of ±0.75 Hz around the 50 Hz nominal value, meaning that frequency deviations within these limits are handled directly by the BESS, which performs the power regulation. Figure 41 presents an FCR-N regulation simulation based on historical frequency data. The frequency data were from December 2025, had

a duration of two hours, and remained within the FCR-N frequency range throughout the entire observation period.

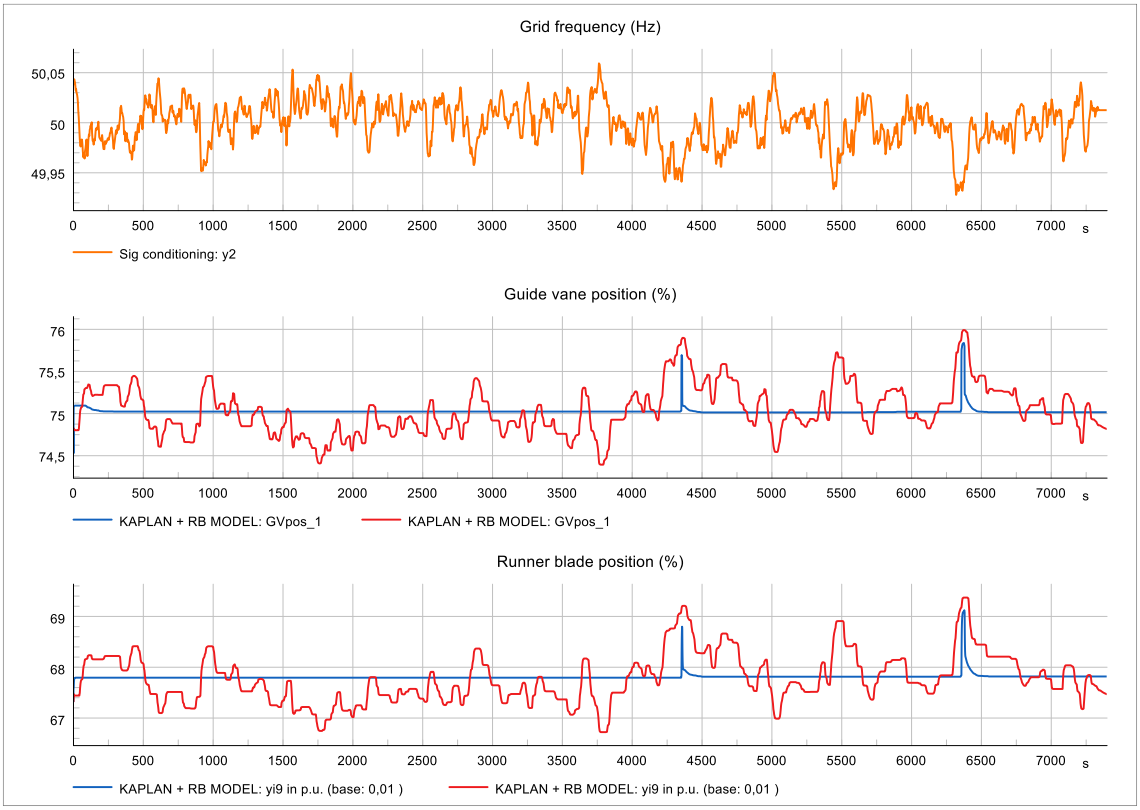


**Figure 41.** Historical frequency data simulation: frequency (orange), model with BESS (blue) and model without BESS (red).

Figure 41 shows how the GV and RB movements behaved with and without the BESS model during the simulation. In the simulation, at approximately 4300 s and 6400 s, the frequency dropped below the allowed limit value, which caused the GV and RB to participate in the regulation.

The GV and RB movements were also compared using Python by applying signal variation calculation. The calculation was performed by exporting simulated historic frequency data results, which stored the GV and RB movements for both the model utilizing the BESS and the model without the BESS over the two-hour simulation period. The calculation was computed by summing the absolute differences between consecutive data

points over the entire observation period with a data sampling interval of 50 ms. The equation used in Python to calculate the GV and RB movements of the plant equipped with the hybrid controller was

$$D_{hybrid} = \sum_{i=2}^{n} |D_i - D_{i-1}|, \tag{32}$$

and

$$D_{n-hybrid} = \sum_{i=2}^{n} |N_i - N_{i-1}|, \tag{33}$$

where $D_{hybrid}$ is the total movement with hybrid control and $D_{n\text{-}hybrid}$ is the total movement without hybrid control. With these equations reduced movement for GV and RB were calculated with equation

$$M = \frac{D_{n-hybrid} - D_{hybrid}}{D_{n-hybrid}} \cdot 100, \tag{34}$$

where *M* is the reduced movement in %. This was performed for both the BESS model and the model without the BESS, after which the results were compared. Based on the Python calculation, in the two-hour FCR-N simulation, the model utilizing the BESS reduced GV movements by 88.28% and RB movements by 89.77%.

# 5 Simulation Results

## 5.1 Turbine Validation

During the turbine validation, the measured GV and RB position signals were applied to the turbine model, which enabled the turbine model to be validated by comparing the simulation response with the measurement data. This ensured that the turbine model was validated using correct position inputs rather than simulated governor outputs.

When validating the turbine model, the most important parameters were the hydraulic head $h_0$ obtained from the measurement data during the test period, the water time constant $T_w$ provided by the turbine supplier, and the parameter $B_{flow}$ which represented the gain describing the impact of blade angle on the turbine water flow. The parameter $B_{flow}$ was optimized together with the fifth-order fitting function, as it was part of the same calculation formula used in the optimization.

During the validation, it was observed that parameters $h_0$ and $B_{flow}$ were directly related to the magnitude of the turbine's active power output, whereas the water time constant $T_w$ primarily affected the phase shift of the active power produced by the turbine model.

As shown in Figure 42, the simulated power matched the measurement data reasonably well in terms of both dynamics and magnitude. Simulations also showed a fast transient at the beginning of the simulation, which settled relatively quickly. This was mainly caused by imperfect initialization of the simulation model.

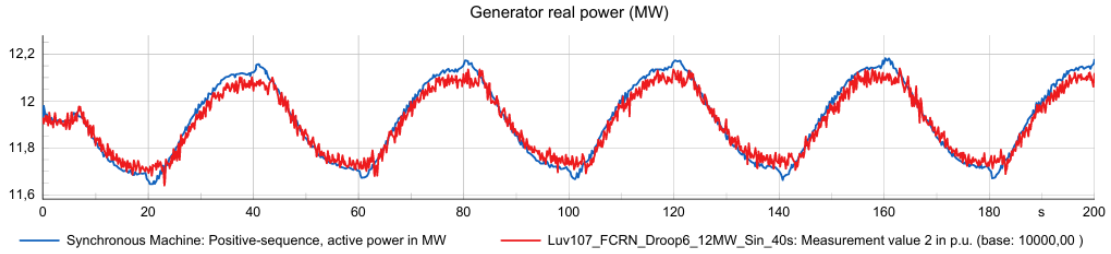


**Figure 42.** FCR-N sine test 40 seconds: generator real power (MW), measured data (red) and simulated response (blue).

The turbine dynamics were strongly influenced by the array GV used in the turbine model, which represented the nonlinearity between the GV and the turbine power output. From the fifth order fitted curve shown in Figure 13, it can be seen how the GV and RB position nonlinearity affected the signal applied to the turbine model. Overall, it was concluded that the nonlinear Kaplan model used in this study was well suited for dynamic simulations and produced sufficiently accurate results with respect to the turbine's active power output and dynamic response. The validated turbine model also provided a solid basis for proceeding to the validation of the turbine governor.

## 5.2 Turbine Governor Validation

The validation of the TG800 turbine governor was challenging due to incomplete site measurement data. In addition to the GV and RB position signals, the validation process would have been more straightforward if the GV and RB position setpoints had also been available. Overall, the simulated turbine governor response showed good match with the site measurement data. However, one mismatch was discovered in the turbine governor implemented in the simulation model. As shown in Figure 43, the GV and RB positions increased to considerably higher values during the 100–400 second periods, after all the generator active power still matched the measurement data well.

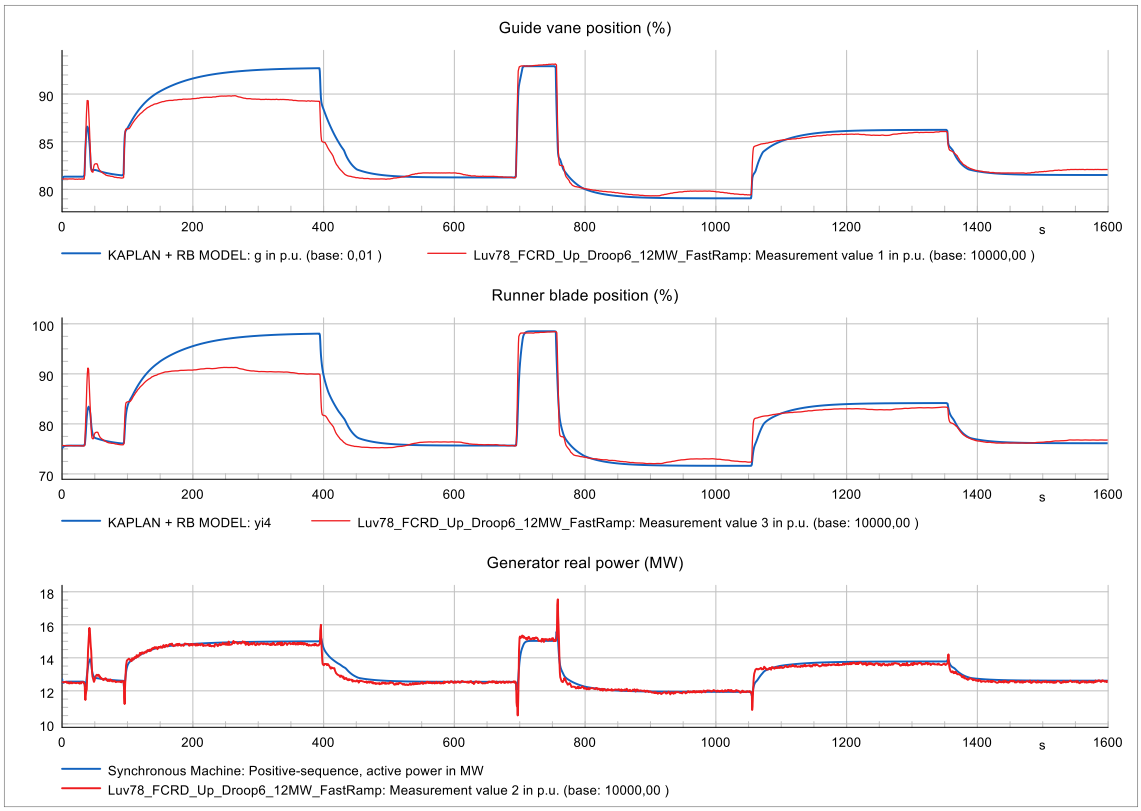


**Figure 43.** FCR-D Up fast ramp test: simulation results (blue) and measurement data (red).

This was likely caused by a discontinuity in the measurement data used to optimize the fifth-order fitted curve in Figure 13. A sudden change in hydraulic head during the recording of the measurement data could have explained the error observed in the simulation model GV and RB positions. Similar behavior was not observed consistently in the other validation cases, which suggested that the issue was related to a specific operating condition. Despite this mismatch, the model simulated the GV and RB position with sufficient accuracy for the purposes of this thesis.

## 5.3 Integrated BESS System

The DIgSILENT BESS template model used in this study was integrated into the TG800 turbine governor in accordance with the ABB document (ABB, 2016a). The impact of the BESS model on the hydropower plant's performance was investigated by simulating FCR-

N tests, in which the frequency signal obtained from the site measurement data was applied to the simulation model. The results obtained from the simulation model were fed into Fingrid's FCP-IT tool, which enabled the assessment of performance and stability. Battery parameters were configured for the BESS model to examine the battery's active-power output and its effect on GV and RB movements during FCR-N provision. This was analyzed by running an approximately two-hour test using Fingrid's historical frequency data.

From the Nyquist curves simulated in the FCP-IT tool, it was observed that the integrated BESS model improved the plant's stability. In particular, stability improvements were obtained in the FCR-N 10 second and 15 second sine tests, which were presented in Section 4.2.1. The performance requirement tests simulated in the FCP-IT tool also demonstrated how the integrated BESS system improved the plant's performance.

In the historical frequency data simulations, the aim was to determine how much the GV and RB position changes could be reduced by using the integrated BESS model while the hydropower plant provided the FCR-N reserve. The approximately two-hour simulation remained within the FCR-N range throughout the entire period, during which the control signal from the Speed Droop exceeded the threshold twice during upward regulation. Based on the simulation results, the extent of the reduction in GV and RB movements achieved through the use of the BESS was calculated. The calculation was implemented using the signal variation equation developed in Python, and the results indicated that the integrated BESS system reduced GV movements by 88.28% and RB movements by 89.77%.

# 6 Discussion and Conclusion

**Question 1:**

How accurately does the developed PowerFactory simulation model represent the dynamic behavior of a hydropower plant when validated against site measurement data?

The validation presented in Sections 5.1 and 5.2 showed that the developed PowerFactory simulation model was able to represent the dynamic behavior of the actual hydropower plant with sufficient accuracy based on the site measurement data. The Kaplan turbine model and the TG800 turbine governor model corresponded to the main dynamic characteristics observed in the measured data, especially in terms of the generator active power output. While some deviations occurred between the simulated and measured responses, the overall behavior of the complete model corresponded well with the measured plant dynamics. Therefore, the developed simulation model can be considered sufficiently accurate for dynamic RMS simulations of hydropower plant operation under FCR-related grid frequency support conditions.

**Question 2:**

How does a BESS integrated into the simulation model's turbine governor affect the power response and stability of a hydropower plant with a slow dynamic response?

For the GV and RB positions, deviations occurred at certain individual data points due to imprecise measurement data. Despite these deviations, the model simulated the generator active power output with sufficient accuracy. The results presented in Section 5.3 showed that the BESS integrated into the simulation model's turbine governor improved the power response and stability of a hydropower plant when the simulations were compared with the site measurement data. The BESS supported the generator active power output by compensating for the slower mechanical response of the turbine, which allowed the plant to respond more quickly to frequency deviations. Also, the BESS improved the stability and performance of the hydro power plant especially in faster

frequency periods. Therefore, the results indicated that integrating a BESS into the turbine governor could support hydropower plants with slow dynamic responses in meeting the current FCR requirements.

**Question 3:**

How much can guide vane and runner blade movements be reduced by integrating a BESS into the turbine governor during FCR-N provision?

The results showed that integrating a BESS into the turbine governor significantly reduced GV and RB movements during FCR-N provision. In the two-hour FCR-N simulation based on historical frequency data, the total movement was calculated by summing the absolute differences between consecutive positions. Compared with the model without BESS, the BESS reduced GV movements by 88.28% and RB movements by 89.77%. This indicated that hybrid control could significantly reduce mechanical control movements during continuous FCR-N regulation and thereby reduce wear and tear in the GV and RB mechanisms.

The aim of the study was to model ABB's TG800 turbine governor with hybrid control together with a Kaplan turbine model. The model was implemented using DIgSILENT PowerFactory software, and the TG800 governor and the Kaplan turbine model were validated in the study. The pre-built DIgSILENT BESS template model used to simulate the hybrid operation was excluded from the validation.

The simulation model was developed to meet the current FCR requirements, and its purpose was to enable simulations of the operation of a hydropower plant during FCR provision. The study examined the operation of the Finnish power system, its frequency control, and the current FCR requirements. To develop the simulation model, the work also discussed the technical aspects of the Kaplan turbine, ABB's TG800 turbine governor, the calculation of FCR capacities, and the characteristics of hybrid control, including the operation and control of the energy storage system.

In future studies, the battery energy storage system in the simulation model could potentially be replaced with a supercapacitor or a flywheel, and SOC management of the energy storage system should be further developed. These developments would allow the suitability of different energy storage technologies for fast frequency support to be compared more thoroughly, while also improving the long-term applicability of the hybrid control strategy.

A second topic for future studies could involve analyzing the economic profitability of an integrated energy storage system in the FCR markets. This could include, for example, the sizing of the energy storage capacity, its type, the investment costs, and the payback period of the investment. In addition, potential savings in maintenance costs resulting from the reduction in GV and RB movements could also be examined.

A third topic for future studies could focus on validating the hybrid control using measurement data from a hydropower plant equipped with an actual energy storage system. This would provide a more accurate assessment of how well the simulated hybrid control corresponds to real plant operation.

# 7 References

ABB. (2016a, April 5). *Simplified Transfer Function Turbine Governor TG800 Hybrid* [Restricted Availability]. ABB.

ABB. (2016b, April 5). *Simplified Transfer Function Turbine Governor TG800 rev B* [Restricted Availability]. ABB.

Åström, K. J., & Murray, R. (2021). *Feedback Systems: An Introduction for Scientists and Engineers, Second Edition*. Princeton University Press.

DIgSILENT GmbH. (2025, April 15). *DIgSILENT Battery Energy Storage System Template*. DIgSILENT Power System Solutions. https://www.digsilent.de/en/powerfactory-download.html

*Electricity system of Finland*. (n.d). Fingrid. https://www.fingrid.fi/en/grid/development/electricity-system-of-finland/

entsoe. (2022, March 15). *Overview of Frequency Control in the Nordic Power System*. Nordic Analysis Group. https://www.epressi.com/media/userfiles/107305/1648196866/overview-of-frequency-control-in-the-nordic-power-system.pdf

*Explanatory document*. (n.d.). Retrieved February 8, 2026, from https://www.svk.se/49720c/siteassets/english/news/1542---explanatory-document-for-the-amended-nordic-synchronous-area-methodology-for-additional-properties-of-fcr.pdf

Feng, C., Mai, Z., Wu, C., Zheng, Y., & Zhang, N. (2024). Advantage of battery energy storage systems for assisting hydropower units to suppress the frequency

fluctuations caused by wind power variations. *Journal of Energy Storage*, *78*. https://doi.org/10.1016/j.est.2023.109989

Fingrid. (2023, September 26). *Reserve products and reserve market places*. https://www.fingrid.fi/globalassets/dokumentit/en/electricity-market/reserves/reserve-products-and-reserve-market-places.pdf

Fingrid. (2025, April 9). *Reserves*. Fingrid. https://www.fingrid.fi/en/electricity-market/reserves/

*Frequency—Historical data*. (n.d.). Retrieved April 15, 2026, from https://data.fingrid.fi/en/datasets/339

Gierling, A. (2025). *Technical Requirements for Frequency Containment Reserve Provision in the Nordic Synchronous Area*. https://www.svk.se/495d28/siteassets/aktorsportalen/bidra-med-reserver/om-olika-reserver/fcr/fcr-technical-requirements_v1.1_28_march_2025.pdf

Gonzalez-Longatt, F. M., & Rueda Torres, J. L. (Eds.). (2021). *Modelling and Simulation of Power Electronic Converter Dominated Power Systems in PowerFactory*. Springer International Publishing. https://doi.org/10.1007/978-3-030-54124-8

*Grid Code Specifications for power-generating facilities VJV2024*. (n.d.). Retrieved December 18, 2025, from https://www.fingrid.fi/globalassets/dokumentit/fi/palvelut/kulutuksen-ja-tuotannon-liittaminen-kantaverkkoon/vjv2024---unofficial-english-translation.pdf

Grigsby, L. L. (2012). *Electric Power Generation, Transmission, and Distribution*. Taylor & Francis Group. http://ebookcentral.proquest.com/lib/tritonia-ebooks/detail.action?docID=911986

Henrique Augusto Menarin, Heliara A. Costa, Guilherme Fredo, & Rodrigo Pereira Gosmann. (n.d.). Dynamic Modeling of Kaplan Turbines Including Flow Rate and Efficiency Static Characteristics. *ResearchGate*. https://doi.org/10.1109/TPWRS.2019.2899815

*Inertia and Rate of Change of Frequency*. (n.d.). Retrieved November 11, 2025, from https://eepublicdownloads.entsoe.eu/clean-documents/SOC%20documents/Inertia%20and%20RoCoF_v17_clean.pdf

Khajeh, H., & Laaksonen, H. (2022a). Potential Ancillary Service Markets for Future Power Systems. *2022 18th International Conference on the European Energy Market (EEM)*, 1–6. https://doi.org/10.1109/EEM54602.2022.9921133

Khajeh, H., & Laaksonen, H. (2022b). Potential Ancillary Service Markets for Future Power Systems. *2022 18th International Conference on the European Energy Market (EEM)*, 1–6. https://doi.org/10.1109/EEM54602.2022.9921133

Koivunen, T., & Syri, S. (2024). Analysis of Severe Scarcity Situations in Finland's Low Carbon Electricity System Until 2030. *Energies*, *17*(23), 5928. https://doi.org/10.3390/en17235928

Kosterev, D. (2004). Hydro Turbine-Governor Model Validation in Pacific Northwest. *Power Systems, IEEE Transactions On*, *19*, 1144–1149. https://doi.org/10.1109/TPWRS.2003.821464

Kuivaniemi, M., Martin, L., & Karlsson, D. (n.d.). *Supporting Document on Technical Requirements for Frequency Containment Reserve Provision in the Nordic Synchronous Area*.

Kundur, P. (1994). Prime Movers and Energy Supply Systems. In *Prime Movers and Energy Supply Systems* (pp. 377–459). McGraw-Hill.

Nordic Analysis Group. (2023, May 29). *Implementation and Tuning Guideline for Fcr Provision*. https://www.fingrid.fi/globalassets/dokumentit/fi/sahkomarkkinat/reservit/implementation-and-tuning-guideline-for-fcr-provision.pdf

Nordic Analysis Group, NAG. (2025). *REQUIREMENTS FOR MINIMUM INERTIA IN THE NORDIC POWER SYSTEM*. https://www.fingrid.fi/globalassets/dokumentit/fi/tiedotteet/2025---requirements-for-minimum-inertia-in-the-nordic-power-system.pdf

Ruokolainen, P. (2016). *Voimalaitosten säätöominaisuudet ja -periaatteet saarekekäytössä*. https://trepo.tuni.fi/handle/123456789/24255

Schäffer, L. E., Korpås, M., & Bakken, T. H. (2023). Implications of environmental constraints in hydropower scheduling for a power system with limited grid and reserve capacity. *Energy Systems*. https://doi.org/10.1007/s12667-023-00594-z

Tibshirani, R. J. (2022). *Divided Differences, Falling Factorials, and Discrete Splines: Another Look at Trend Filtering and Related Problems* (arXiv:2003.03886). arXiv. https://doi.org/10.48550/arXiv.2003.03886

Valtonen, M., & Lehtovuori, A. (2017). *Piirianalyysi, osa 2*.

Zhao, J., Wang, L., Liu, D., Wang, J., Zhao, Y., Liu, T., & Wang, H. (2015). Dynamic Model of Kaplan Turbine Regulating System Suitable for Power System Analysis. *Mathematical Problems in Engineering*, *2015*, 1–12. https://doi.org/10.1155/2015/294523